Evidence of active subglacial lakes under a slowly moving coastal region of the Antarctic Ice Sheet

Jennifer F. Arthur[1], Calvin Shackleton[1], Geir Moholdt[1], Kenichi Matsuoka[1], Jelte van Oostveen[2]

[1]Norwegian Polar Institute, 9296 Tromsø, Norway
[2] NORCE Norwegian Research Centre, 9294 Tromsø, Norway
Correspondence to: Jennifer Arthur (jennifer.arthur@npolar.no)

Abstract

Active subglacial lakes beneath the Antarctic Ice Sheet provide insights into the dynamic subglacial environment, with implications for ice-sheet dynamics and mass balance. Most previously -identified lakes have been found upstream (>100 km) of fast-flowing glaciers in West Antarctica, and none in the coastal region of Dronning Maud Land (DML) in East Antarctica. The regional distribution and extent of lakes as well as their timescales and mechanisms of filling-draining activity remain poorly understood. We present local ice surface elevation changes in the coastal DML region that we interpret as unique evidence of seven active subglacial lakes located ~~near the~~under slowly -moving ice near the grounding line~~-sheet~~ margin. Laser altimetry data from the ICESat-2 and ICESat satellites combined with multi-temporal REMA strips reveal that these lakes actively fill and drain over periods of several years. Stochastic analysis of subglacial water routing together with visible surface lineations on ice shelves indicate that these lakes discharge meltwater across the grounding line. Two lakes are within 15 km of the grounding line, while another three are within 54 km. Ice flows 17-172 m a^{-1} near these lakes, much slower than the mean ice flow speed near other active lakes within 100 km of the grounding line (303 m a^{-1}). ~~Our observations add to a previously under-represented population of subglacial lakes that exist beneath slow-flowing ice near the ice sheet margin.~~ Our results improve knowledge of subglacial meltwater dynamics and evolution in this region of East Antarctica and provide new observational data to refine subglacial hydrological models.

1 Introduction

Hydrologically -active subglacial lakes periodically store and release water beneath the Antarctic Ice Sheet and form a key component of the basal hydrological system. Active lakes are known to influence the dynamics of the overlying ice by reducing basal friction and periodically triggering short-term accelerations in ice flow (Stearns et al., 2008; Siegfried et al., 2016; Siegfried and Fricker, 2018; Andersen et al., 2023). Temporary accelerations in ice flow of up to ~10% have been linked to lake drainage events on Byrd Glacier, East Antarctica (Stearns et al., 2008), on Crane Glacier, the Antarctic Peninsula (Scambos et al., 2011), and on the Mercer and Whillans ice streams, West Antarctica (Siegfried et al., 2016). Individual active

subglacial lakes can range from ~5 km^2 to ~~tens~~ thousands of square kilometres and have been shown to form connected networks over hundreds of kilometres (Fricker et al., 2007, 2009; Smith et al., 2009; Flament et al., 2014; Siegfried and Fricker, 2018; Hodgson et al., 2022; Livingstone et al., 2022). Downstream subglacial water flow has been linked to cascading lake drainage events which transport excess water episodically towards the grounding line (Flament et al., 2014; Smith et al., 2017; Siegfried and Fricker, 2018; ~~Smith et al., 2017;~~ Neckel et al., 2021). Meltwater outlets at the grounding line discharge freshwater into sub-ice-shelf cavities, which according to models could enhance ice-shelf basal melting (Carter and Fricker, ~~2017~~2012; Dow et al., 2022) and reduce sea-ice volume (Goldberg et al., 2023) and has also been shown to influence sediment fluxes (Lepp et al., 2022) and biogeochemical fluxes (Wadham et al., 2013). Therefore, observing active lakes using repeated satellite data is crucial to characterize subglacial hydrology and its impact on the ice-sheet-ocean system.

Over the past two decades, over 140 active subglacial lakes have been detected underneath the Antarctic Ice Sheet using satellite data (Fig. 1, Neckel et al., 2021; Livingstone et al., 2022). Satellite radar and laser altimetry (e.g., ESA's CryoSat-2 and NASA's Ice, Cloud and Land Elevation Satellites ICESat and ICESat-2) has successfully been used to identify localised ice surface elevation changes on annual to decadal timescales, interpreted as subglacial lake filling and draining activity and corresponding changes in lake volume (e.g., Fricker et al., 2007, 2010; Smith et al., 2009). Even finer patterns of centimetre-scale ice surface elevation changes have been identified using differential synthetic aperture radar interferometry (DInSAR) and interpreted as evidence for transient subglacial water transport (Gray et al., 2005; Neckel et al., 2021; Moon et al., 2022). Few active subglacial lakes have yet been reported ~~beneath much of the grounded ice close to~~in the coastal region of the Antarctic Ice Sheet ~~margin~~ (Livingstone et al., 2022). Specifically, only ten active lakes have been previously identified within 50 km of the ice-sheet grounding line (Livingstone et al., 2022). Consequently, little is known about the subglacial hydrology, water routing and the impact on local ice dynamics at the transition between grounded and floating ice in this region.

In this study, we build on previous work by providing a more complete inventory of active subglacial lakes inferred from ~~by~~ measuring ice surface elevation displacement ~~observed from~~using the laser altimeters onboard ICESat-2 between March 2019 and May 2023 and its predecessor ICESat between October 2003 and March 2009. We focus on the coastal Dronning Maud Land (DML) region of East Antarctica, where no active lakes have been identified previously (Fig. 1). We use ICESat and ICESat-2 elevation time series together with strip data from the Reference Digital Elevation Model of Antarctica (REMA; Howat et al. 2019) ~~strips~~ to determine the temporal patterns of subglacial lake activity and estimate lake volume changes. We further estimate subglacial stream probability using water routing analyses derived from stochastic simulation (Shackleton et al., 2023) to assess upstream ~~drainage basins~~ hydrological systems and potential downstream impacts of the newly observed subglacial lakes. The combination of these datasets reveals seven previously ~~-~~unreported active subglacial lakes that fill and drain over periods of multiple years and identifies the most probable pathways of meltwater released from lakes towards the grounding line. Our study provides insights into ~~an~~ active subglacial hydrological systems and potential subglacial outlets ~~close to the ice sheet margin~~ in the coastal region ~~in~~ of eastern Dronning Maud Land. This can help to better constrain how

subglacial lake activity regulates ~~water availability and flow conditions under the ice sheet~~ ice-sheet basal conditions and ice dynamics, as well as modifies ice-shelf cavity circulation and basal melting when meltwater is released at the grounding line.

2 Study Area, Data and Methods

2.1 Study Area

~~In the Dronning Maud Land (DML) sector of East Antarctica, previous work has identified a cluster of eight ice surface subsidence and uplift events between 2017-2020 ~160 km inland from Jutulstraumen Glacier using double differential synthetic aperture radar interferometry (DDInSAR) and ICESat-2 altimetry (Neckel et al., 2021). These vertical movements of the ice surface reached 14.4 cm and were interpreted as episodic subglacial lake drainage events with durations between 12 days and ~1 year, indicating cascading subglacial water over a ~175 km flow path (Neckel et al., 2021). The DML coastal region is also characterized by sparse radar-detected, stable subglacial lakes. Goeller et al. (2016) found 33 locations with distinct characteristics in airborne ice-penetrating radar data that can be interpreted as subglacial lakes 40 km or further inland from the grounding line (7.2-16.2° E). So far, no active subglacial lakes have been recorded in the coastal region of DML within 160 km of the ice margin.~~ We focus on the coastal region of grounded ice in DML, extending along the Princess Astrid Coast and the Princess Ragnhild Coast up until the Roi Baudouin Ice Shelf (69° S to 72° S and 33° W to 6° E; Fig. 1). There are ~13 fast-flowing outlet glaciers along this coast (88 – 281 m a^{-1}), which are surrounded by slowly moving ice (2-30 m a^{-1}, Gardner et al., 2018). Grounded ice in this region of the ice sheet lies largely below present-day sea level (Morlighem et al., ~~2020~~2022; Frémand et al., 2023, Fig. 1). Satellite altimetry from ICESat/ICESat-2 has recorded significant ice-sheet thickening in DML over the last two decades (Smith et al. 2020) due to high snowfall rates (e.g. Boening et al., 2012). So far, no active subglacial lakes have been recorded in the coastal region of DML, but ~160 km inland near the onset of Jutulstraumen ice stream, west of our study region, a cluster of eight ice surface subsidence and uplift events between 2017-2020 were identified using double differential synthetic aperture radar interferometry (DDInSAR) and ICESat-2 altimetry (Neckel et al., 2021). These vertical movements of the ice surface reached 14.4 cm and were interpreted as episodic subglacial lake drainage events with durations between 12 days and ~1 year, indicating cascading subglacial water over a ~175 km flow path (Neckel et al., 2021). Stable subglacial lakes have also been detected from airborne ice-penetrating radar data at 33 locations in the inland of DML (Fig. 1, Goeller et al., 2016). In contrast to hydrologically active lakes which fill and drain over decadal or shorter timescales, stable subglacial lakes predominantly detected from radio-echo sounding beneath the warm-based ice-sheet interior tend to be stable over >103 year-timescales (Wright and Siegert, 2012; Livingstone et al., 2022).

2.2 Satellite Altimetry

2.2.1 ICESat-2

NASA's next generation Ice, Cloud, and land Elevation satellite (ICESat-2) is a photon-counting laser altimeter providing repeat-pass ice surface height measurements every 91 days (Markus et al., 2017). The Advanced Topographic Laser Altimeter System (ATLAS) on board ICESat-2 continuously profiles the Earth's surface along its 1387 reference ground tracks (RGTs) using six laser beams, which measure three pairs of tracks, with each pair separated by 3.3 km. The beams within each pair are separated by ~90 m. Elevation-change data in this paper are based on release 6 of the ICESat-2 Level 3b Slope-Corrected Land Ice Height time series (ATL11) product (Smith et al., ~~2022~~2023a) which became available in August 2023. We used the ATL11 data spanning between April 2019 and April 2023, for which the geolocation of each beam is accurately determined (Smith et al., 2023b). We omitted the ATL11 data collected between October 2018 and March 2019, because an issue with the central beam pair pointing resulted in displacement of ICESat-2 measured tracks from the RGTs by up to several kilometres (Smith et al., 2023b). All previous studies detecting subglacial lakes in Antarctica from ICESat-2 have used the lower-level ICESat-2 ATL06 product, which provides geolocated, land-ice surface heights that are corrected for geophysical impacts and instrument bias (e.g. Siegfried and Fricker, 2021; Neckel et al., 2021; Fan et al., 2022).

A main difference between ATL06 and ATL11 is that ATL06 elevations require slope correction using a DEM or data-fitted reference surface when comparing repeat-tracks, whereas this is already done as part of the ATL11 processing, directly providing time series of along-track ice surface heights that are slope-corrected onto a reference pair track (RPT) for each cycle and are accurate to <0.07 m (Smith et al., ~~2019~~2023b; Brunt et al., 2021). In this way, ATL11 height estimates have corrected ATL06 heights for the combined effect of small cross-track offsets (up to ~130 m) between repeat measurements and sub-kilometre and surface topography around fit centres. The ATL11 product has so far been used in Antarctica for assessing the impact of net snow accumulation variability on observed surface height change (Medley et al., 2022) and for investigating ice-shelf basal channel morphology at the Kamb Ice Stream grounding line (Whiteford et al., 2022). Over the Greenland Ice Sheet, ATL11 has been used for evaluating spatial patterns of surface mass balance and firn densification (Smith et al., 2023b) and for investigating subglacial lake activity beneath the surface ablation zone (Fan et al., 2023).

Two types of height error estimates are provided with ATL11. One is random per-point estimates (*h_corr_sigma*), which include the errors related to the accuracy of the reference surface and the precision of the ICESat-2 range estimates and are uncorrelated between adjacent reference points (Smith et al., 2023b). The other is systematic error estimates (*h_corr_sigma_systematic*), which include the slope-dependent impact of geolocation errors that are correlated along each track. We find maximum per-point error and systematic error in the corrected surface heights of 14.9 cm and 14.5 cm respectively for the ICESat-2 data we analyse here. These maximum values are higher than reported per-point errors in the ice-sheet interior of 1-2 cm, because rougher, steeper surfaces towards the coast typically degrade the instrument precision and

slope correction (Smith et al., 2023b). However, the mean per-point and systematic errors for the ICESat-2 data analysed here are still as low as 2.7 cm and 5.3 cm, respectively.

To investigate subglacial lake drainage and filling patterns, we followed the approach of calculating repeat-track elevation anomalies (Fricker et al., 2014, Neckel et al., 2021; Siegfried and Fricker, 2018; 2021). We first removed poor-quality surface elevations, potentially caused by cloud cover, blowing snow or background photon clustering based on ATL11's overall quality summary flag (*atl11_qual_summary* == 0) (Siegfried and Fricker, 2021). Previous studies have calculated elevation anomalies with respect to a DEM or other reference surface (Fricker et al., 2014; Neckel et al., 2021). Using the slope-corrected ATL11, we assessed ice surface elevation changes directly with respect to the start of our observation period (April 2019) by calculating elevation anomalies (dh) for each ATL11 point along every RGT relative to the first available cycle (h_0) using: $dh = h - h_0$, where h is ice surface elevation. We calculated time series of elevation anomalies along each RGT.

2.2.2 ICESat

NASA's Ice, Cloud, and land Elevation satellite (ICESat) was a laser altimeter providing ice surface height measurements in footprints of ~65 m-diameter separated by ~172 m along its RGTs (~~Zwally et al., 2002~~Schutz et al., 2005; Fricker and Padman, 2007). We used ICESat GLA12 ice-sheet product version 34 collected between February 2003 and October 2009 to derive elevation changes. ICESat RGTs were typically repeated within ~150 m cross-track distance, and vertically accurate within a few tens of centimetres depending on surface slope (Brenner et al., 2007; Kohler et al., 2012). ICESat crossover errors (i.e. at the point where successive ascending and descending passes intersect ~~at the point between successive ascending and descending passes over the same location~~) have been estimated between 7.5 cm for flat surfaces to 20 cm for 1° slopes (Smith et al., 2009), meaning most errors are <~~0.1~~ 15 cm ~~given the minimal surface slopes over most of the Antarctic Ice Sheet (Smith et al., 2009).~~in our study region where slopes are typically <0.6° (Smith et al., 2009). The GLA12 product was used for compiling the first comprehensive Antarctic inventory of 124 active subglacial lakes north of 86° S, demonstrating short-term basal hydrologic evolution of lakes throughout Antarctica (Smith et al., 2017).

We estimated along-track elevation changes from GLA12 following the approach of Moholdt et al. (2010) by fitting surface planes to 700 m segments of repeat track data, determining surface elevation anomalies for all laser footprints with respect to the plane fit. Outlier points with elevation anomalies >10 m, for example due to cloud scattering or rough topography, were iteratively removed in the plane-fit processing. This threshold was set higher than the expected elevation changes due to subglacial lake activity, in order to not remove such data. We further neglected potential long-term elevation changes due to surface mass balance and large-scale ice dynamics in the plane fitting as these are generally an order of magnitude smaller ~~small in the study region~~ (Pratap et al., 2022; Goel et al., 2024) than the elevation anomalies we observe ~~and could interfere with changes~~ due to subglacial lake activity.

2.3 Subglacial lake detection

Previous studies have identified lakes based on thresholds between ±0.1-0.5 m for spatially-coherent elevation anomalies using ICESat (Fricker et al., 2007, 2014; Smith et al., 2009) and Cryosat-2 (Kim et al., 2016; Smith et al., 2017, Malczyk et al., 2020). We adapted these previous approaches to our coastal study region, which is characterized by high slope and roughness, by identifying potential areas of subglacial lake activity from ICESat/ICESat-2 repeat-tracks with significant (±1 m) elevation anomalies over a distance of ≥1 km. The elevation anomaly patterns over these areas were then manually examined to assess whether these appeared to reflect lake activity (i.e., arc-shaped profiles of draining and/or filling) or if they were in, for example, highly-crevassed or sloping regions where unresolved rough topography is likely to dominate the signal. We found that using a ±1 m threshold applied to elevation anomalies relative to the start of our observation period best highlighted and distinguished substantial localised anomalies from background along-track elevation changes and noise, whereas lower thresholds (e.g. ±0.5 m) included surface elevation change signals that are unlikely to be related to subglacial lake activity.

2.4 REMA sStrip dDifferencing and lake outlines

Following detection of ICESat-2 surface elevation anomalies, we used high-resolution stereoscopic data from REMA (Howat et al., 2019) over these locations to further investigate subglacial lake activity and spatial extents. We differenced available DEM strips with 2-m map cells acquired between September 2015 and December 2021 that intersected regions with elevation anomalies identified in ICESat/ICESat-2 data to calculate surface height changes over three suspected lakes (L1, R1, R2: Table 1). ~~To further investigate subglacial lake activity and spatial extents, we used high-resolution stereoscopic data from REMA (Howat et al., 2019) over the locations where we detected ICESat-2 anomalies in surface elevation change. We differenced available DEM strips with 2-m map cells acquired between September 2015 and December 2021 that intersected regions with elevation anomalies identified in ICESat/ICESat-2 data to calculate spatial ice surface height changes over three suspected lakes (L1, R1, R2: Table 1).~~ The number of useable DEM strips (i.e. partially or fully covering each lake) in any given year averaged between 1 and 3 strips per lake (Supplementary Fig. 1). The strip DEMs are generated by applying fully-automated, stereo auto-correlation techniques to overlapping pairs of high-resolution optical satellite images, using the open-source Surface Extraction from TIN-based Searchspace Minimization (SETSM) software (Howat et al., 2019). Individual 2-m REMA strips are not co-registered to satellite altimetry, unlike the REMA mosaic (Howat et al., 2019), meaning that relative elevation within a strip is precise but has low absolute accuracy (Hodgson et al., 2022). To increase absolute accuracy, DEM strips can be coregistered using static reference points, typically rock outcrops (Shean et al., 2019). The strips we used do not include any outcrops, so instead we estimated and removed vertical elevation biases by using the temporally closest overlapping ICESat-2 track within +/- 100 days of the DEM strip acquisition date (Chartrand and Howat, 2020; Priergaard Zinck et al., 2023). This time restriction ensures that the ~~ICESat-2~~REMA elevations are representative for the ~~of elevations during~~ strip acquisition time, although we acknowledge that some lake filling or drainage could still occur within this time period.

Of the ten DEM strips that intersected the seven potential areas of subglacial lake activity we identified, six strips were vertically co-registered to ICESat-2 elevations (Supplementary Table 1). The other four strips were not co-registered due to lacking contemporaneous ICESat-2 data, but were still included to provide further insight into the lake activity of Lakes L1 and R1 (Supplementary Fig. 2). In these cases, the remaining vertical biases are reflected in near-constant elevation differences outside of the active lake areas. Static lake boundaries were digitized from the pattern of elevation anomalies in the REMA difference maps (Lakes L1, R1 and R2). We were unable to estimate the areas of four lakes (M1, M2, V1, R3) because the REMA strip differences did not show any significant elevation anomalies. For illustrative purposes, we still sketched speculative lake boundaries for these four lakes (Fig. 2d-e) based on ICESat-2 elevation anomaly locations and the REMA mosaic hillshade (Howat et al., 2019).

2.5 Subglacial lake volume changes and recharge rates

To estimate lake volume changes, we multiplied the REMA-derived lake areas (where available) with the altimetry-based median elevation anomaly within this lake boundary for each repeat track (Smith et al., 2009; Carter et al., 2011). We approximated subglacial water flux by the volume change corresponding to ice surface uplift/deflation over time (Malczyk et al., 2020, 2023). Recharge rates (reported as annual water supply to each lake) were estimated by applying linear regression against volume change and time during the refilling (inter-drainage) period, following Malczyk et al. (2020). We were unable to estimate volume changes for the five lakes without a clear or complete lake boundary in the REMA data. In the absence of further constraints on lake extent changes over time, we assume a constant lake area throughout the fill-drain cycle and a constant overlying ice thickness (Fricker and Scambos, 2009), even though migrating lake boundaries through fill-drain cycles can impact the estimated lake volume changes (Siegfried and Fricker, 2021).

2.6 Hydropotential Subglacial Water Flow Mapping

To interpret the satellite-detected lake activity in the context of the broader hydrological system under the ice sheet, we mapped potential subglacial water drainage pathways and their uncertainty based on an ensemble of bed elevation grids generated through stochastic simulation (~~water routing analyses following the approaches of~~ MacKie et al. (~~2020, 2021~~); ~~and~~ Shackleton et al.~~,~~ (2023). We made a 1 km grid for the DML region, limited to ca. <73° south to save computation time, and used ~~We made a 1 km grid for the DML region, limited to ca. <73° south to save computation time, and calculated the probability of each grid cell to contain subglacial streams. We did this by first generating 50 equally-likely bed topography grids with continuous, realistic roughness simulated between radar-derived ice thickness measurements using a sequential Gaussian simulation algorithm (MacKie et al., 2023). I~~ice thickness data from Frémand et al. (2023) ~~were used~~ as a basis for the simulations, after filtering out surveys conducted before 1990 which have limited locational accuracy~~. , and converting to b~~Bed elevations were calculated ~~data~~ by subtracting ~~it~~ ice thicknesses from ice ~~extracted~~ surface elevations extracted ~~of~~ from the 500 m REMA mosaic product (Howat et al. 2019), and~~.~~ w~~W~~e also added elevation data from rock outcrops at pixel centroids ~~of the REMA 500 m grid (Howat et al. 2019)~~. To model measurement variance accounting for spatially varying characteristics

of the bed ~~W~~we chose to ~~divided~~cluster the ~~region~~ data into 12 regions ~~clusters~~(Supplementary Fig. 3~~X~~) using a k-means clustering algorithm on measurement coordinates (MacKie et al., 2023). ~~and calculated t~~The experimental variogram was calculated using the SciKit-GStat python package (Mälicke, 2022) for normalised ~~measurements~~bed elevation values in each cluster, giving measurement variance for increasing lag distance in each region. ~~which w~~We ~~used to fit~~ found best-fitting~~a~~ statistical models and parameters for each region based on a least-squares analysis for exponential (clusters 0,5,6,9,11), spherical (clusters 1,2,3,4,8,10), and Gaussian (cluster 7) model fits (Supplementary Fig. 3~~X~~).

~~representing measurement variance at increasing lag distances in each regional cluster (Mälicke, 2022). This was done to sequentially~~We generated an ensemble of 50 equally-likely bed elevation grids using a sequential Gaussian simulation algorithm from the GStatSim python package (MacKie et al., 2023), which simulate~~s~~e ~~values~~ bed elevations between measurements along a randomized path over the domain, ~~by~~ picking from a Gaussian distribution conditioned at each grid cell by the closest 50 bed elevation measurements and modelled variance. ~~The resulting ensemble of 50 bed elevation grids were then used to estimate subglacial hydraulic potential (ϕ) following Shreve (1972).~~ We ~~also~~ used the median absolute deviation (MAD) between the 50 ~~simulated bed elevation~~ grids as a measure of bed elevation uncertainty. Low MAD is associated to regions with a high data density and lower basal roughness, whereas high MAD occurs for large distances ~~between~~ to the nearby survey profiles and in regions with high basal roughness where there is greater potential for bed elevation variability between measurements (Shackleton et al., 2023). Figure 1b shows where the MAD is lower than 100 m, indicating regions of relatively low bed uncertainty and higher confidence in simulated subglacial water routing.

The simulated ~~ensemble of 50~~ bed grids ~~elevation grids were~~were used together with REMA ice surface elevations (Howat et al., 2019) to estimate gridded ice thicknesses and calculate subglacial hydraulic potential (ϕ) following Shreve (1972), which corresponds to each simulated bed. We assumed that water pressure equals ice overburden pressure, and ~~calculated~~ predicted water routing ~~for~~ along hydraulic potential gradients assuming a spatially uniform melt rate ~~based on a depression-filled bed topography~~ using a D∞ algorithm (Tarboton, 1997). Subglacial stream probability was calculated ~~based on~~from the number of ~~predicted~~ streams predicted per grid cell over the ensemble of simulated bed ~~topography~~~~elevation grids~~. This ~~method~~ approach provides uncertainty-constrained water routing predictions where uncertainty can be sourced either from a lack of measurements (i.e. topography is not known well-enough), lack of strong topographic control on water flow, or both. Low probability streams are therefore associated to regions with sparse data or in flat areas where water routing is sensitive to minor fluctuations in bed elevation between simulations. We similarly derived the probability of subglacial hydrological catchment boundaries using the drainage basins for streams predicted in water routing analyses over the simulated bed. We then ~~further~~ estimated the ensemble-average upstream ~~subglacial hydrological~~ catchment area potentially draining towards ~~for~~ each altimetry-detected lake ~~, based on the average upstream watershed area generated from our water routing analyses and derived catchment boundary probabilities based from the ensemble on the 50 stochastic simulations~~ (Supplementary Fig. ~~6~~4).

3 Results

3.1 Observed ice surface displacements and interpreted lake activity

We identify seven locations with significant (>1 m) anomalous, repeated surface elevation changes over distances of a kilometre or more from ICESat/ICESat-2 repeat tracks, which we interpret as active subglacial lakes. Lake R1 is located 19 km upstream from the Roi Baudouin Ice Shelf grounding line and is crossed by two intersecting ICESat-2 tracks and one ICESat track that all show a ~5-km wide elevation anomaly (Fig. 2a, Table 1). Lake L1 is 32 km upstream of the Lazarev Ice Shelf and is crossed by two ICESat tracks and two ICESat-2 tracks (Fig. 2b). Lake R2 is 115 km inland from the Roi Baudouin Ice Shelf and is crossed by only one ICESat-2 track (Fig. 2c). Lake V1 is located 54 km upstream of the Vigridisen Ice Shelf and is crossed by two intersecting ICESat-2 tracks (Fig. 2d). Lakes M1 and M2 are only 10 km apart, and 5 km and 15 km upstream of the Muninisen Ice Shelf, respectively (Fig. 2e). Lastly, Lake R3 is 136 km inland from the Roi Baudouin Ice Shelf and is crossed by one track (Fig. 2f), which shows a ~7-km wide elevation anomaly (Supplementary Fig. ~~3d~~5d).

Following Smith et al. (2009), we classify 'high-confidence' active lakes as being detected from elevation anomalies in at least two intersecting reference tracks, and lakes that are only identified from one satellite altimetry track as 'provisionally active'. By this definition, five of the lakes (R1, L1, V1, M1 and M2) are classified as high-confidence, and two (R2 and R3) as provisionally active. However, we can independently detect localised elevation anomalies over Lake R2 from REMA strip differencing, supporting that this is an actively filling and draining lake. Three of the seven lakes were confirmed and delineated by REMA strip differencing during 2019-2021 (Fig. 4; L1, R1, R2) and two of these also had intersecting ICESat tracks to extend the change record back to 2003-2009 (Fig. 3 and 5; L1 and R1). Their lake areas range from 21.5 to 40.1 km^2 (Table 1). The other four lakes (V1, M1, M2, R3) had no ICESat data and no detectable change between REMA strips, likely due to negligible elevation changes between the dates covered by the strips.

All seven active lakes are located below sea level and beneath ice thicknesses of 800-1500 m (Fig. 1b). These lakes are typically located in relatively slow-flowing regions: two lakes under 20 m a^{-1}, three lakes between 60-90 m a^{-1}, and two beneath slightly faster-flowing tributaries at 152 and 172 m a^{-1} (Fig. 1b, Table 1). The lakes located close to ice flow divides are beneath especially slow-flowing ice, for example Lake L1 (Fig. 1b, Table 1). The lakes upstream of Vigridisen and Muninisen ice shelves are located beneath faster-flowing outlet glaciers (up to 170 m a^{-1}; Gardner et al., 2018).

We assume a one-to-one ratio between ice surface elevation changes and lake volumetric change, following previous studies in Antarctica and Greenland (Smith et al., 2009, Malczyk et al., 2023, Fan et al., 2023). It is possible that some ice surface uplift and subsidence could be influenced by ice-flow dynamics, blowing snow and changes in basal traction, resulting in misinterpretation as subglacial lake activity (Sergienko et al., 2007; Humbert et al., 2018), so this relationship lacks precise quantification (Siegfried and Fricker, 2018). For example, in fast-flowing regions, surface-elevation changes can reflect ice-

flow changes triggered by water displacement at the bed during lake drainage (Smith et al., 2017). Most of the lakes in this study are beneath relatively slow-flowing ice (< 100 m a^{-1}), making it unlikely that observed ice surface changes resulted from ice flowing into basal topographic depressions. The patterns of surface elevation change we observe are characteristic of subglacial lake drainage (i.e. deepening towards the lake centre) and lack uplift near localised subsidence, which can be a signal of ice dynamical changes (Carter and Fricker, 2012). We also note that lake widths (inferred from elevation anomaly widths) are large relative to ice thickness (e.g. L1: ~8.5 ice thicknesses, R1: ~4 ice thicknesses), whereas ice-dynamical effects tend to dominate only when lakes are small relative to ice thickness (Fricker and Scambos, 2009). Ice surface changes over our newly-identified lakes (up to 4.5 m) are much larger than those related to wind-driven snow redistribution and firn compaction, typically <0.5 m a^{-1} based on repeat-track elevation changes elsewhere in the region. Furthermore, the spatial co-occurrence between altimetry- and REMA-derived elevation anomalies and predicted subglacial stream locations (Section 3.3) gives us confidence that subglacial meltwater drains towards the observed lakes and that elevation changes are therefore due to subglacial lake activity rather than other surface changes. Therefore, we conclude that the ice surface elevation changes we observe reflect changes in water volume rather than ice dynamics and surface processes, although we acknowledge that actual lake volume changes are still uncertain due to potential migration of lakeshore boundaries through fill-drain cycles (Siegfried and Fricker, 2021).

3.1.1 Lake L1 upstream of Lazarevisen

Over Lake L1 we find steady ice surface subsidence between August 2020 until May 2023 (Fig. 3d-f), suggesting a lake drainage event over a period of at least 2 years and 8 months. This is preceded by a slight ice surface uplift between May 2019 and May 2020, indicating lake refilling. REMA data show slight subsidence beside these tracks during September 2015 – December 2016 and January 2020 – February 2021, suggesting overall lake volume loss during these two periods (Fig. 4c, Supplementary Fig. ~~1b~~2b). This is consistent with the time series of lake volume derived from ICESat-2, showing the lake steadily draining between May 2020 and May 2023 (Fig. 3f). Elevation anomalies along the two intersecting ICESat tracks continue for 5 km along Track 134 and 7 km along Track 215, reaching a maximum value of 3 m at the lake centre (Fig. 3d-e, Supplementary Fig. ~~4a~~6b). The lake-averaged elevation anomaly time series over Lake L1 (Fig. 5) reveals positive elevation anomalies from November 2003 to March 2007 followed by a large (> 3 m) subsidence over the next 1 year and 8 months, indicating lake drainage. Ice surface displacements show a distinct minimum at the lake centre that tapers out towards the lake edges.

3.1.2 Lakes R1, R2 and R3 upstream of Roi Baudouin

The time series of elevation anomalies from ICESat-2, ICESat and REMA strip differencing show variable drain and/or fill patterns for these three lakes over the past two decades (Figs 3 and 5). The elevation time series for Lake R1 shows negative anomalies up to -2.4 m in December 2019, followed by a gradual elevation increase to up to 4.5 m in March 2023 (Fig. 3a-b), likely representing ~~). We interpret this as ice surface subsidence in response to~~ lake drainage~~,~~ followed by ~~uplift in response to~~

~~the~~ lake filling over the next 3 years and 5 months. This is consistent with observed elevation gain (lake filling) from REMA differencing between October 2019 and January 2021 (Fig. 4a). Earlier REMA data indicate a slight subsidence (lake drainage) between December 2016 and December 2017 (Supplementary Fig. 2a), just ahead of the ICESat-2 observed subsidence in 2019. Time series of lake volume change shows the lake steadily filling between April 2019 and March 2022 (Fig 3c). More than a decade earlier, ICESat repeat tracks show a steady subsidence across the same area between 2003 and 2009 (Fig. 5, Supplementary Fig. ~~4b~~6a), ~~which we interpret as~~ a sign of lake draining. ICESat-2 data show that Lake R2 was draining between May 2019 and April 2021, and has since been filling through to April 2023 (Supplementary Fig. ~~3c~~5c). The shape of the lake can be seen from a distinct pattern of uplift between two REMA strips from January 2021 and December 2022 (Fig. 4b). Lastly, over Lake R3 we find ~~continuous~~ gradual ice surface uplift from August 2019 to April 2023 in response to lake filling (Fig. 5).

3.1.3 Lakes V1, M1, M2 upstream of Vigridisen and Muninisen

We record gradual subsidence up to -1.6 m ~~ice surface subsidence~~ over Lake V1 from August 2019 to May 2023, ~~which we interpret as continuous~~ indicating a slow lake drainage (Fig. 5, Supplementary Fig. ~~3a~~5a). ~~We find continuous~~A gradual lake filling over 4 years is apparent from ice surface uplift along a ~2.5-km wide zone of Lake M1 from May 2019 until May 2023~~, suggesting lake filling over 4 years~~ (Fig. 5, Supplementary Fig. ~~3b~~5b). Likewise at Lake M2, lake refilling is found to occur over a ~3 year and 8-month period ~~we found continuous~~as indicated by ice surface uplift along a ~3-km wide elevation anomaly from September 2019 to June 2023~~, indicating lake refilling during this ~3 year and 8-month period~~ (Fig. 5, Supplementary Fig. ~~3b~~5b). There is a striking coherence between the filling rates of these two lakes during the ICESat-2 period. Without any further intersecting altimetry tracks or clear change patterns in REMA strips for these lakes, it is difficult to constrain their areas and volume changes. The lack of significant localised elevation changes from REMA differencing could be because they had just drained and not yet refilled in the period covered by the DEM strips, or that draining and refilling have roughly balanced each other.

3.2 Subglacial lake volume changes, recharge rates and water flux

We calculated annual water supply and recharge rates for lakes R1 and L1, where lake boundaries were fully delineated from REMA strip differencing (Fig. 4). Lake R1 steadily gained volume from December 2019 to January 2023 before starting to drain (Fig. 3c, Fig 5). The associated volume gain of 0.13 km^3 over 3.5 years corresponds to a yearly recharge rate of 0.03 km^3 a^{-1}. Lake L1 gained 0.01 km^3 volume between February 2020 and August 2020 before starting to drain until May 2023 (Fig. 3f). During this half-year period, Lake L1 recharged at a rate of 0.02 km^3 a^{-1}. Similarly -sized active lakes have been suggested to recharge at similar rates to those reported here, for example Lake Cook E2 (46 km^2, 0.05 km^3 a^{-1}) and Lake Whillans 2b (25 km^2, 0.02 km^3 a^{-1}) (Li et al., 2020; Malczyk et al., 2020). Our estimated lake volume gains and losses are of similar magnitude to the median lake volume change of ~0.12 km^3 for 140 active lakes around Antarctica based on their surface elevation histories

(Livingstone et al., 2022). However, since we are unable to capture a full drainage or filling cycle for most lakes, actual lake volume changes between minimum and maximum states are likely higher than what we can capture.

To approximate the subglacial meltwater flux entering/leaving the largest lake we detected (Lake L1), we calculated the rate of volume change corresponding to ice surface uplift/deflation over time (Malczyk et al., 2020). We use Lake L1 as an example for estimating water flux, as it is located close to the ~~ice margin~~grounding line where topographic uncertainty is relatively low, and has one of the smallest mean upstream catchment areas (0.9 x 10^4 km^2, Table 1). Average subglacial water flux was 4.9 m^3 s^{-1} between November 2003 and May 2023. For comparison, Malczyk et al. (2020) estimated an average water flux of 141 m^3 s^{-1} in 2013 for a network of active lakes upstream of Thwaites Glacier (Thw_{70}, Thw_{124}, Thw_{142} and Thw_{170}). Modelled upstream melt supplies to their lake network range from 0.04-0.17 km^3 a^{-1} (1.3-5.4 m^3 s^{-1}) although these lakes are considerably larger than those in our study (up to 484 km^2; Smith et al., 2017). In our water flux estimations, we assume no lake outflow during lake filling, though it is possible a lake could increase in volume whilst discharging water downstream if a high lake influx exceeds lake outflow (Carter and Fricker, 2012). These assumptions mean that our estimated water flux is likely to be a minimum estimate.

3.3 ~~Subglacial water flow~~Predicted subglacial water routing

We simulated an ensemble of 50 equally-likely bed elevation grids using sequential Gaussian simulation (Supplementary Fig. ~~Y~~7: Simulations 1-3). The resulting grids are consistent along survey profiles and have continuous, regionally representative roughness simulated between measurements. Throughout the ensemble, water routing analyses predict dendritic networks of subglacial streams routing water from inland towards the grounding line (Supplementary Fig. ~~5~~8). This broad pattern of drainage remains consistent over the ensemble, but the kilometer-scale routing of meltwater varies. Stream probability maps (Fig. 1a) show water flow predictions strongly controlled by bed topography in the inland mountain regions where radar measurements are limited but nevertheless outcrop surface elevation data help constrain ~~the bed topography~~water routing. High stream probability coincides with dense radar survey coverage, for example surrounding the Nivlisen Ice Shelf, showing the impact of data density on reducing water routing uncertainty. Lower stream probability regions that resemble ~~diffuse~~discontinuous, spatially-distributed streams occur between higher-probability streams, for example inland of the Roi Baudouin Ice Shelf eastward of 27° E (Fig. 6e) and inland of the Muninisen Ice Shelf, often coinciding with widely-spaced radar survey profiles. Other regions show inconsistent water routing despite regularly-spaced radar profiles, such as within 50 km of the Vigridisen grounding line (Fig. 1a). This reflects an absence of strong topographic features that control the routing of water, ~~meaning~~ so that small differences in simulated ~~topography~~ elevations over the ensemble can reroute water and lead to inconsistent water routing and more diffuse stream predictions.

We compared our lake observations with the subglacial drainage patterns and found good spatial correspondence over some of the lakes. Predicted water routing shows direct drainage to the western Roi Baudouin Ice Shelf grounding line and identifies

likely subglacial outlet locations (Fig. 6a). Lake R1 aligns with several known subglacial water conduits detected at the grounding line in airborne ice-penetrating radar data that align with two sub-ice-shelf channels (Fig. 6a, Drews, 2015; Drews et al., 2017; 2020). This agreement indicates that Lake R1 is likely to be discharging subglacial meltwater ~~directly~~ into the ice-shelf cavity through a channelized subglacial conduit system and could contribute to a meltwater plume that forms the sub-ice-shelf channel. However, Lake R1 is 6 km from the closest radar survey profile, and our subglacial stream probabilities highlight that precise drainage routes are less certain here since topographic uncertainty is high (MAD > ~~over~~ 125 m) in the middle of adjacent radar survey profiles (Fig. 6a). Given the topographic uncertainty in this region, we cannot rule out the potential for lake drainage towards different outlets, for example if ephemeral subglacial channels close between drainage events. Several ice-shelf channels on Roi Baudouin aligned to ice flow direction correspond with the predicted subglacial meltwater outlets beneath the grounded ice sheet and align with the location of Lakes R2 and R3 (Fig. 6e). Therefore, Lakes R2 and R3 could discharge basal water that is routed towards multiple subglacial outlets at the Roi Baudouin grounding line.

Further west, the probability map of subglacial drainage catchments (Supplementary Fig. ~~6~~4) shows with high confidence that an extensive catchment of minimum 19,000 km^2 is draining towards Lake V1. Downstream water routing predictions vary too much at the kilometre-scale to conclusively determine ~~ice margin~~ outlet locations at the grounding line, and water routing shows drainage towards the grounding lines of either Vigridisen Ice Shelf or the neighbouring Fimbulisen Ice Shelf (Fig. 6b). Inland of Lazarevisen Ice Shelf, predicted subglacial stream and outlet locations become more uncertain, reflecting sparser radar profile spacing (up to 19 km), but suggest Lake L1 likely discharges meltwater to the Lazarevisen Ice Shelf grounding line (Fig. 6c). Our water routing analyses also predicts high-probability streams connecting Lakes M1 and M2, suggesting interconnected lakes which drain ~~directly~~ into the ice-shelf cavity (Fig. 6d). The predicted subglacial outlet here is close to several sub-ice-shelf channels, indicating Lakes M1 and M2 feed a persistent sub-shelf channel when they drain.

4 Discussion

4.1 Lake distributions ~~at~~ in the coastal region of the Antarctic ice ~~-~~sheet ~~margin~~

We identify seven previously undocumented active subglacial lakes in coastal DML at six localities ~~in five different drainage basins and~~ within 5 km of the ice-sheet grounding line, feeding into separate ice shelves (Fig. 1a). The combination of ICESat, ICESat-2 and REMA observations presented here build upon large-scale repeat satellite altimetry studies of hydrologically ~~-~~ active subglacial lakes elsewhere in Antarctica (e.g., Fricker et al., 2007, 2009; Smith et al., 2009; Siegfried and Fricker, 2021). Only ten active lakes have been identified previously within 50 km of the Antarctic-wide grounding line for the rest of Antarctica (Livingstone et al., 2022). These ten known lakes nearby the grounding line are found on the Antarctic Peninsula (1 lake), inland of Totten Glacier (2 lakes), and inland of the Rutford (1 lake), Mercer (2 lakes), Whillans (3 lakes) and Kamb ice streams (1 lake) (Scambos et al., 2011; Wright and Siegfried, 2012; Siegfried and Fricker, 2018).

The location of our identified subglacial lakes demonstrate that thicker, fast-flowing upstream ice is not a pre-requisite for active subglacial lake existence at least in this part of East Antarctica. All seven lakes are located below sea level and below ice thicknesses of 812-1524 m (Table 1; Fig. 1b). In contrast, the mean ice thickness ~~of~~ over previously ~~-~~reported active lakes in Antarctica is 2272 m (Livingstone et al., 2022). The newly detected lakes are generally located beneath slow-flowing ice (<65 m a^{-1}) (Fig. 1b). This contrasts with most known active lakes within 100 km of the Antarctic grounding line that lie beneath fast-flowing ice (>200 m a^{-1}; Gardner et al., 2018; Livingstone et al., 2022). Two exceptions are Lakes KT2 (31.7 km^2) and KT3 (38.7 km^2) beneath the Kamb Ice Stream, which are comparable in area to our Lakes L1 and R1 (31-38 km^2) and are located under near-stagnant ice (<2 m a^{-1}) (Kim et al., 2016; Siegfried and Fricker, 2018). Another exception is the active lake system beneath Haynes Glacier in West Antarctica, where ice flow speed is ~131 m a^{-1} (Hoffman et al., 2020). Ice thickness above these ~~three~~ four lakes (820 – 1845 m) is within a similar range to our lakes (828-1503 m, Table 1). Much of the grounded ice along the Antarctic ~~ice margin~~coast is slow-flowing (<200 m a^{-1}) and lies below sea level within a similar ice thickness range. Consequently, moderately-sized ~~near margin~~ active subglacial lakes in the coastal region, similar to the ones presented here at 1-10 km in length and at least 20 – 40 km^2, are likely under-represented in Antarctic-wide inventories, yet could store and release significant volumes of water. Large volumes of water stored and released by these subglacial lakes could regulate downstream ice flow (Siegfried et al., 2016) and control the location of subglacial ~~ice margin~~ water outlet~~s locations~~at the grounding line, driving sub-ice shelf circulation and melting that could impact ice-shelf stability (e.g. Jenkins et al., 2011, Gwyther et al., 2023).

That these lakes are located so close to the ~~ice margin~~ice-sheet grounding line beneath relatively slowly ~~-~~flowing ice is unexpected, since the ice-sheet bed is predicted to be cold beneath large parts of the Antarctic coastal region (Pattyn, 2010). ~~since thick ice and low surface mass balance at inland regions of Antarctica are typically associated with thawing ice sheet bed where geothermal heat flow and ice flow speeds are low (Pattyn et al., 2016).~~ In contrast, thawing ice-sheet bed is typically associated with low geothermal heat flow and ice flow speeds beneath thick ice and low surface mass balance at inland regions of Antarctica (Pattyn, 2010; Pattyn et al., 2016). However, the presence of these lakes in coastal DML indicates ~~that there are~~existence of temperate basal conditions where meltwater is accumulating either in situ or is sourced from pressure changes upstream that trigger drainage further downstream along a channelized subglacial system (Hoffman et al., 2020; Neckel et al., 2021; Dow et al., 2022). The ensemble analyses of bed topographies indicate that the detected lakes have large potential upstream catchments, ranging from 0.5 x10^4 km^2 (R1) to 2.3 x10^4 km^2 (V1; Table 1). For lakes located beneath slow-flowing ice, upstream subglacial meltwater supply is primarily controlled by geothermal heat flow (Malczyk et al., 2020) and model results suggest grounded basal ice across DML is at the pressure melting point (Pattyn, 2010). Therefore, lake recharge is likely regulated by geothermal heat flow, not by frictional heat generated by fast-flowing ice streams or outlet glaciers. The spatial distribution of our lakes can be used to constrain estimates of geothermal heat flow by calculating the minimum geothermal heat flow needed to keep the ice-sheet base at pressure melting point at the lake locations (Wright ~~et al.,~~and Siegert, 2012). Given that our estimated lake recharge rate for Lake R1 is 0.03 km^3 a^{-1} and the subglacial drainage catchment is 0.5

x10^4 km^2, the mean basal melt rate required over the ~~basin~~ catchment to fill Lake R1 can be approximated as 0.03 km^3 a^{-1} / 0.5 x10^4 km^2 = 6 mm a^{-1}. Similarly, for Lake L1 the required basal melt rate can be approximated as 2.2 mm a^{-1}. This is within a reasonable range for coastal DML, where ice sheet model experiments have su~~1~~ggested that the mean basal melt rate can reach up to 10 mm a^{-1} beneath grounded ice (Pattyn, 2010).

None of the newly detected lakes in this study are beneath ice experiencing extensive surface meltwater production or ponding (Arthur et al., 2022; Mahagaonkar ~~and Moholdt, 2022~~et al., 2024), meaning surface meltwater reaching the ice bed can be discounted as a potential influence on subglacial lake recharge/behaviour. However, we discounted a ~1.8 km-wide surface elevation anomaly 5 km inland of the Nivlisen Ice Shelf grounding line ~~was discounted~~ as subglacial in origin because large volumes of supraglacial meltwater are known to pond and flow onto the ice shelf in this region (Dell et al., 2020~~; Arthur et al., 2022~~). Extensive supraglacial lake activity can produce large local apparent elevation change that can be misclassified as subglacial lake activity, although it is possible for subglacial lake drainage to create an ice-surface depression that provides a natural basin for surface meltwater to pond (Fan et al., 2023). Additionally, perennial buried lake drainage close to the grounding line can also produce surface elevation change signatures on the order of several metres. Approximately 40 km west of Lake R1, Dunmire et al. (2020) detected an average ice surface lowering of ~2.5 m over 1 year and 8 months due to draining of a buried lake ~~draining~~, and Sentinel-1 data indicated that the lake drained again three years later. In contrast, our results show that ice surface uplift and lowering over the seven subglacial lakes occurs over multi-year timescales, with a longer cyclicity (~2-5 years).

One possible consideration for the two lakes closest to the grounding line (<16 km, M1 and M2) is that the observed elevation anomalies along these four ICESat-2 tracks reflect seawater intrusion ~~in~~ from the ice-shelf grounding zone. Tidal migrations of seawater intrusions up to 20 cm thick along subglacial troughs over timescales of several weeks have been reported from Sentinel-1 differential InSAR up to 15 km upstream of the Amery Ice Shelf grounding line (Chen et al., 2023). Robel et al. (2022) also showed with numerical modelling that seawater intrusion over impermeable beds may occur up to tens of kilometres upstream of grounding lines. However, t~~t~~he magnitude of observed elevation anomalies at M1 and M2 (>2 m ice surface uplift) and the multi-year timescale of these changes indicates lake filling rather than intrusion of a centimetre-scale seawater sheet. The predicted presence of subglacial sedimentary basins in coastal DML suggests a permeable ice-sheet bed, meaning seawater intrusion is unlikely (Li et al., 2022).

4.2 Lake filling and draining patterns

We show that the seven lakes fill and drain over periods of several years (Fig. 3, Fig. 5). This is consistent with observations from ICESat and ICESat-2 measurements elsewhere in Antarctica, where lakes ~~continuously~~ drain or fill over 3 or 4 years (e.g. Fricker and Scambos, 2009; Fricker et al., 2007; Smith et al., 2009). Similarly, Livingstone et al. (2022) reported lakes in

Antarctica exhibiting extended multi-year periods of ~~quiescence (filling)~~ filling and draining, based on the ratio of ~~filling (~~ice surface uplift~~)~~ and ~~draining (~~ice surface subsidence~~)~~ of ~~known~~ previously identified active lakes.

The limited spatial coverage, observational frequency and duration of ICESat, ICESat-2 and REMA make it challenging to determine the frequency of lake fill-drain cycles and to resolve potential rapid, episodic lake drainages on daily to monthly timescales. There might also be some undetected smaller lakes as ICESat-2 repeat track spacing is up to 9 km in coastal DML, while the smallest lakes we recorded were 5 km wide. Smaller, centimetre-scale surface expressions of lake activity or seawater intrusion on shorter timescales require more detailed or sensitive data like InSAR (Neckel et al., 2021). For example, Neckel et al. (2021) showed that eight lakes of comparable size (7-51 km^2) inland of the ice stream Jutulstraumen ~~Glacier~~ drained in a cascade over 12 days to ~5 months. Consequently, the short-term dynamics and hydrological networks of the new lakes we report may be under sampled, as they could also form interconnected, cascading systems.

4.3 Subglacial water flow

The agreement between our subglacial lake locations, predicted subglacial drainage pathways and ice-shelf channels indicates that these lakes are actively discharging subglacial meltwater through a channelized subglacial conduit system in coastal DML, likely routing subglacial water ~~directly~~ into ice-shelf cavities. Previously, this link was made for active lakes beneath fast-flowing ice streams e.g. beneath the MacAyeal Ice Stream and Thwaites Glacier in West Antarctica (Fricker et al., 2010, Smith et al., 2017). Further work should compare simultaneous observations of ice surface height anomalies and ice velocity changes to constrain how the subglacial hydrological system co-evolves with subglacial lake fill-drain activity and to determine the influence on ice-shelf dynamics in coastal DML. Similar investigations have been conducted for a series of subglacial drainage events along the Northeast Greenland Ice Stream using Sentinel-1 DInSAR (Andersen et al., 2023) and Thwaites Glacier using Sentinel-1 and GNSS (Hoffman et al., 2020).

Our probability analysis of subglacial water routing shows increased uncertainty in drainage pathways downstream of Lakes V1, L1, R1 and R2 (Fig. 6c-f), mainly due to sparse radar survey coverage in these regions. Also, subglacial channels in these regions could ~~also~~ be ephemeral and only form during lake drainage events (Smith et al., 2017)~~., and~~ W~~w~~ithout strong topographic drivers of water flow it is possible that the routing of meltwater and outlet locations could be variable between drainage events which could affect the location of subglacial meltwater outlets and consequently local sub-ice-shelf circulation and melt rates. Our analysis highlights regions where more densely-spaced radar profiles are needed to reduce uncertainty in basal topography and water routing, for example inland of the Roi Baudouin Ice Shelf and Lazarev Ice Shelf grounding lines. International coordinated programmes like RINGS (Matsuoka et al., 2022; scar.org/science/cross/rings) involving new radar data collection along and inland of the Antarctic grounding line should help to close this knowledge gap.

5 Summary and Outlook

We identified seven local surface height anomalies of magnitudes up to ±4 m using repeated ICESat-2 records in coastal DML, which we interpret as active subglacial lakes. The largest of these lakes was ~9 km long and ~5 km wide. ICESat laser altimetry and REMA strip differencing were used to extend the elevation change time series over three of these lakes. We detected multiple long-term lake fill-drain cycles from ICESat and ICESat-2 repeat tracks, which coincide spatially with elevation anomalies from differenced REMA strips. Six of the seven lakes coincide with predicted subglacial drainage systems using an ensemble of stochastically-simulated bed topographies that consider potential bed roughness between survey profiles. The combination of these datasets indicates that the hydrologically -active lakes fill and drain over several years and are linked to channelized subglacial drainage routing meltwater towards the grounding line ~~in coastal DML~~. In contrast to previously detected subglacial lakes that are typically located under fast-flowing or thicker inland ice, the newly detected lakes are found beneath slower-flowing (17-172 m a^{-1}) ~~grounded~~ ice near the ~~ice margin~~grounding line, with implications for ice-sheet dynamics and freshwater discharge beneath ice shelves. Our results improve knowledge of subglacial meltwater dynamics in this region of East Antarctica and provide new observational data to refine subglacial hydrological models, for example for validating predicted lake and stream locations. ~~This~~ Such refinements are~~is~~ crucial to accurately capture the complexity of dynamic basal conditions and their impact on ~~to~~ ice-sheet dynamics.

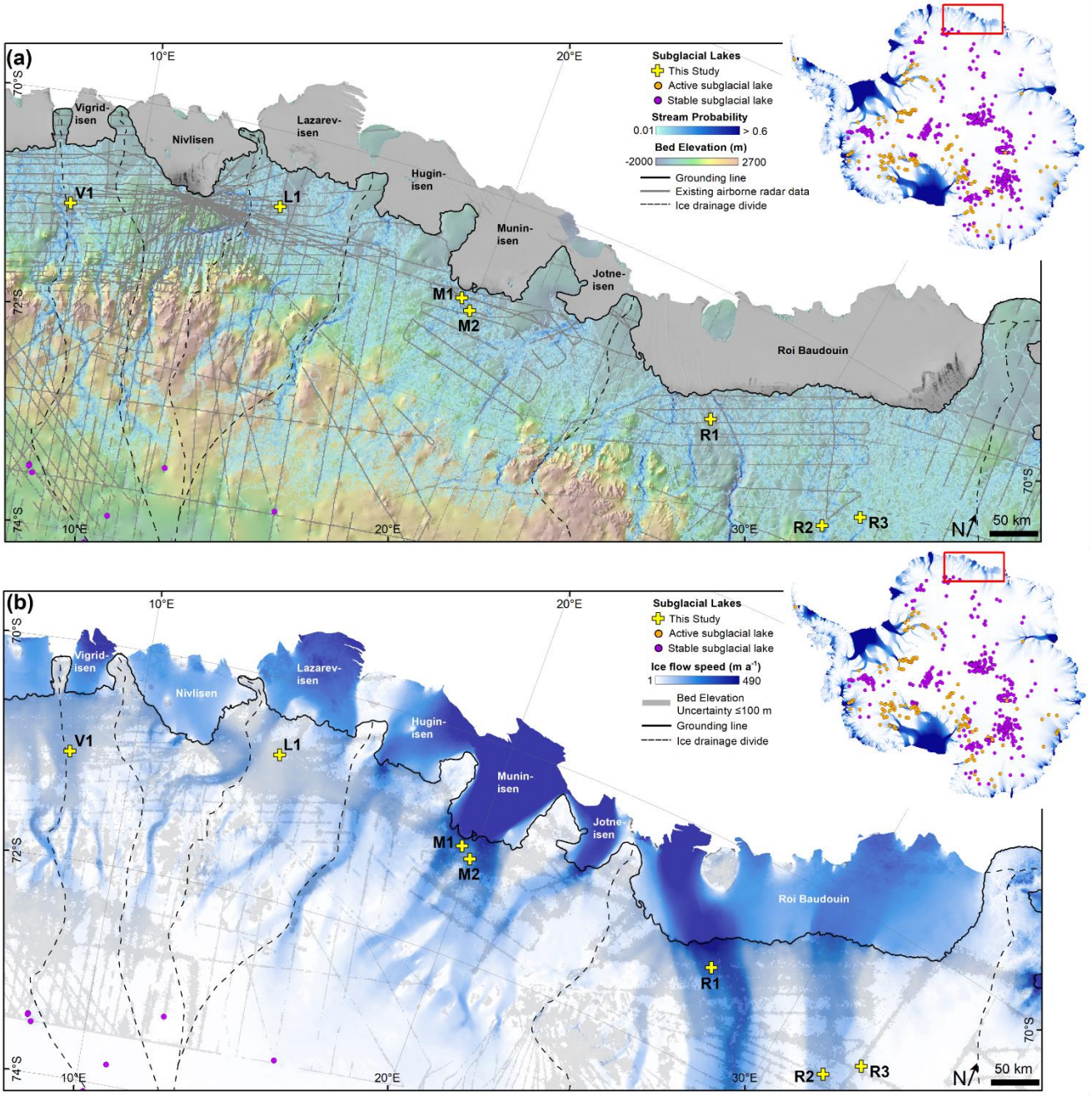

Figure 1: The coastal region in Dronning Maud Land. (a) The locations of active subglacial lakes identified in this study in relation to predicted subglacial stream locations based on water routing analysis, bed topography and regional radar data availability. The ~~dashed~~ black solid line is the MEaSUREs grounding line (Rignot et al., 2016), bed elevations are from BedMachine (Morlighem et al., 2022), radar data availability is from Frémand et al. (2023), and the ice flow drainage divides (dashed lines) are from Mouginot et al. (2017). Subglacial lake locations in the inset map are from Livingstone et al. (2022), where active lakes are represented by orange dots and stable lakes by ~~green~~ purple dots. (b) Ice flow speed (Gardner et al., 2018) in blue shading and areas with bed elevation uncertainty <100 m based on the median absolute deviation between 50 bed topography simulations in this study (all other regions ≥100 m). Simulations of subglacial water drainage pathways are limited to ca. <73° south.

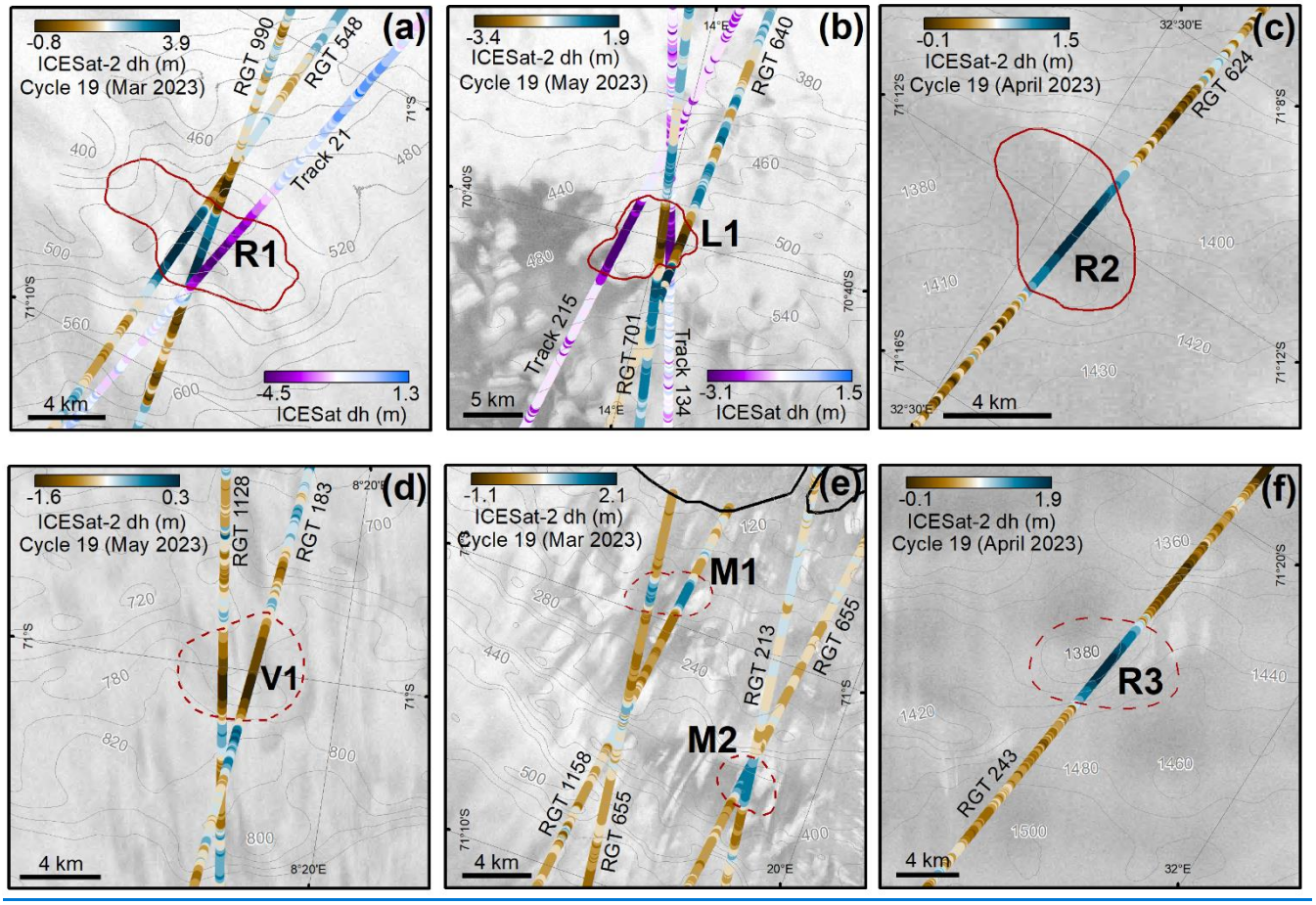

Figure 2: Along-track surface elevation anomalies for each detected subglacial lake, indicating ice surface subsidence (subglacial lake draining) or uplift (subglacial lake filling). ICESat-2 reference ground tracks (RGTs) shown in Panels a-f and ICESat tracks shown in Panels a and b. Inferred lake boundaries derived from REMA differencing (Panels a, b and c~~;~~) are shown as ~~black dashed~~ red solid lines~~)~~, while manually delineated lake boundaries ~~or manual delineation~~ (Panels d, e, f~~;~~) ~~purple~~ are shown as red dashed lines~~.) are shown as dashed black outlines.~~ Ice flow direction is represented by black arrows (Gardner et al., 2018). Contours represent surface elevation from REMA (Howat et al., 2019). The bold black line in Panel (e) is the MEaSUREs grounding line (Rignot et al., 2016). Other observed ice surface elevation changes do not meet the > 1 m anomaly criteria for active lakes (Section 2.~~5~~3). Background image is the RADARSAT mosaic (Jezek et al., 2013).

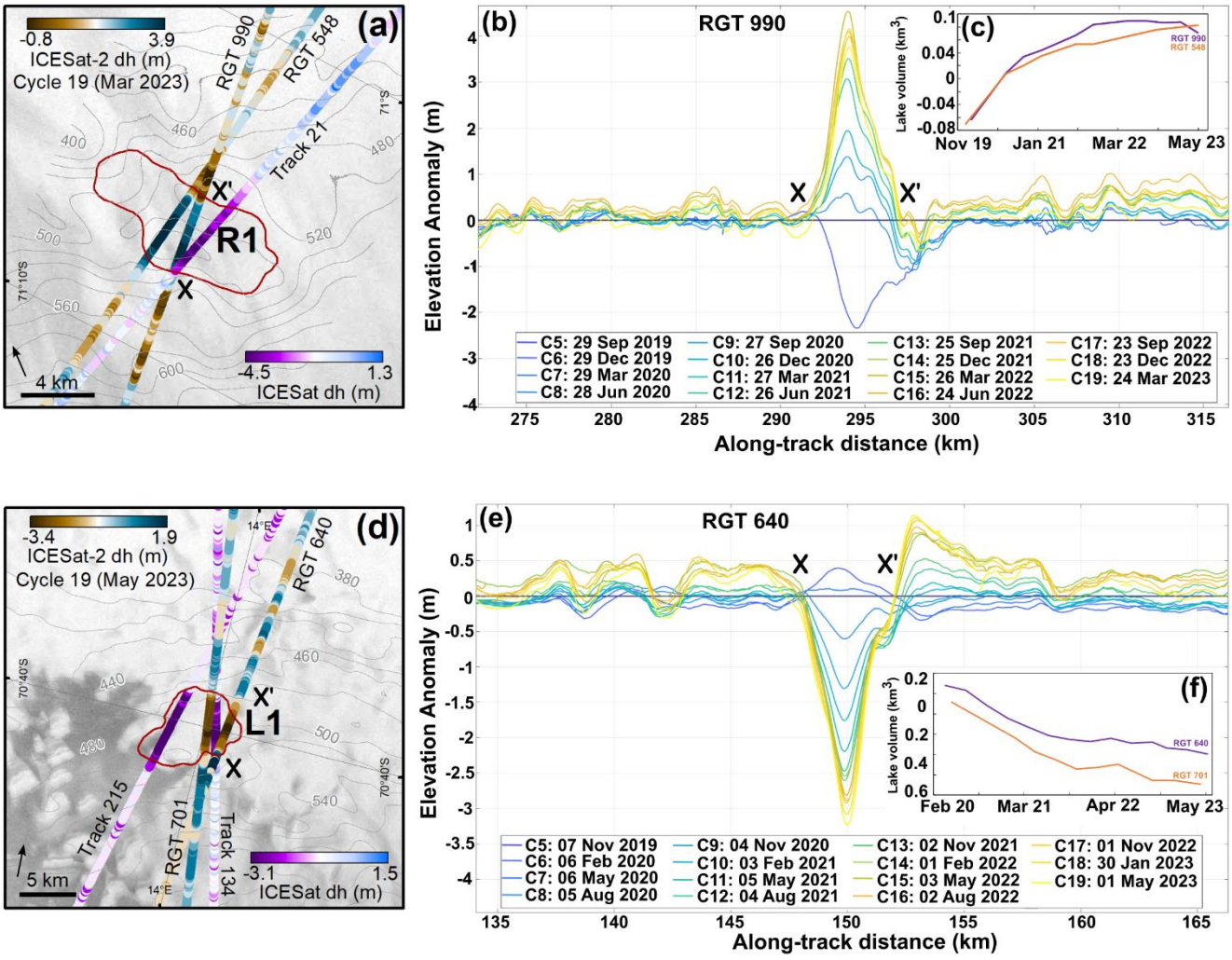

Figure 3: Ice surface elevation displacements for an actively filling lake (Lake R1, a-c) upstream of the Roi Baudouin Ice Shelf and an actively draining lake (Lake L1, c-e) upstream of the Lazarev Ice Shelf, both derived from ICESat-2 and ICESat. Significant (>1 m) ice surface elevation anomalies along ICESat-2 reference ground tracks (RGTs) are highlighted by X-X' in each panel. Panels (b) and (e) show ice surface elevation displacements relative to ICESat-2 Cycle 3 (April/May 2019). Ice surface elevations from Cycle 4 are not plotted as these were removed by the data quality flag during initial data filtering. Colours correspond to each individual ICESat-2 cycle. Panels (c) and (f) show time series of estimated lake volume.

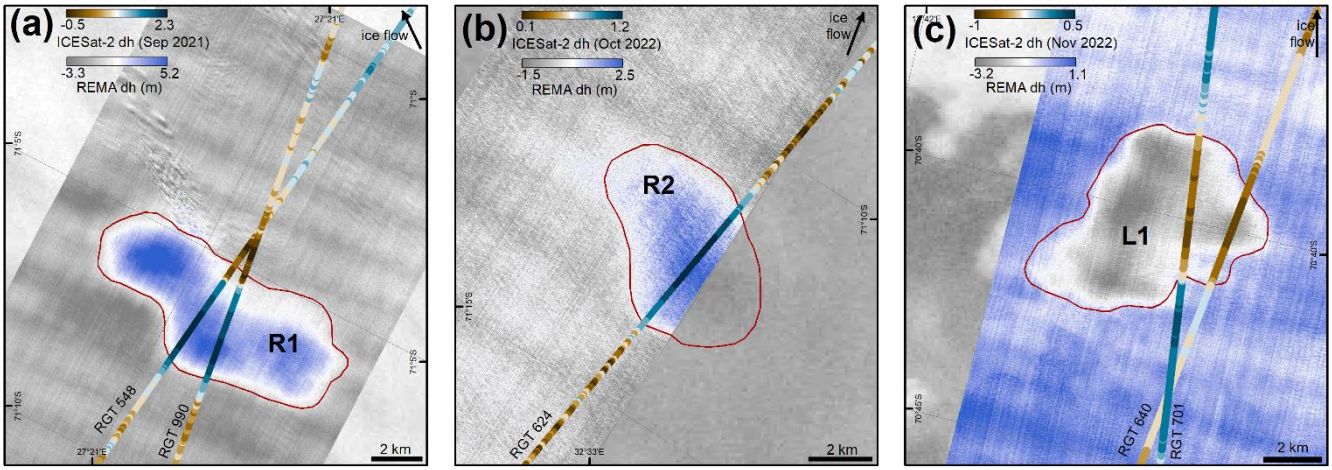

Figure 4: Ice surface elevation change from REMA strip differencing. (a) Lake R1, and (b) Lake R2, both upstream of the Roi Baudouin Ice Shelf. (c) Lake L1 upstream of the Lazarev Ice Shelf. ICESat-2 elevation changes are relative to April 2019 (a) and May 2019 (b, c). Regions of localised elevation anomaly (blue shading for uplift and yellow shading for subsidence) between REMA strip pairs (22nd October 2019 – 10th January 2021 in Panel a, 18th January 2021 – 28th December 2022 in Panel b, 25th January 2020 – 15th February 2021 in Panel c) are delineated by the ~~dashed~~ red lines. These boundaries were outlined manually based on visual assessment. Each example highlights the spatial co-occurrence between significant localised ice surface uplift/subsidence and surface elevation anomalies along the intersecting ICESat-2 reference ground tracks (RGTs). The slight offset between the localised elevation anomalies in the ICESat-2 RGTs~~tracks~~ and the REMA difference map over Lake R1 in Panel (a) could be due to lake boundary migration since the date of the REMA strip (January 2021).

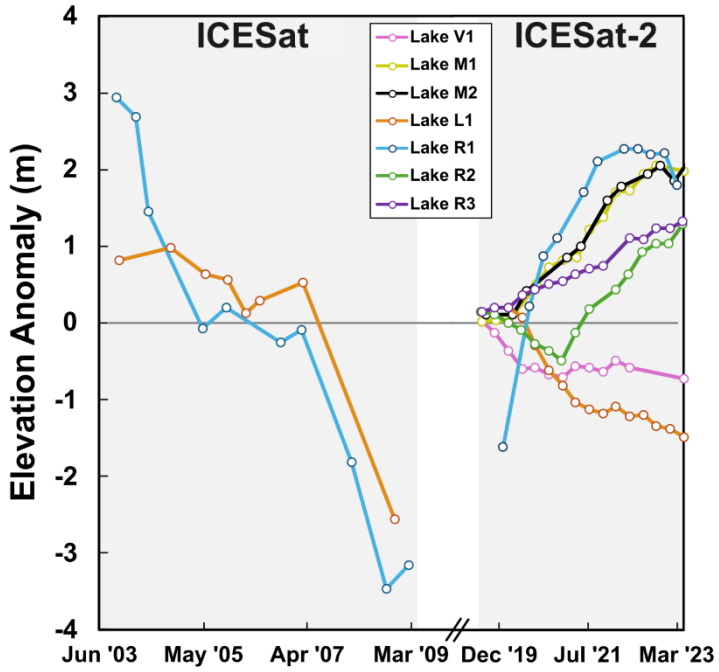

Figure 5: ICESat and ICESat-2-derived ice surface elevation time series (calculated as median elevation anomalies within each lake boundary with respect to elevations in the first available cycle). Lakes L1, R1 and R2 use lake boundaries derived from REMA differencing and Lakes V1, M1, M2 and R3 use boundaries based on locations of significant (>1 m) elevation anomalies over a distance of a kilometre or more.

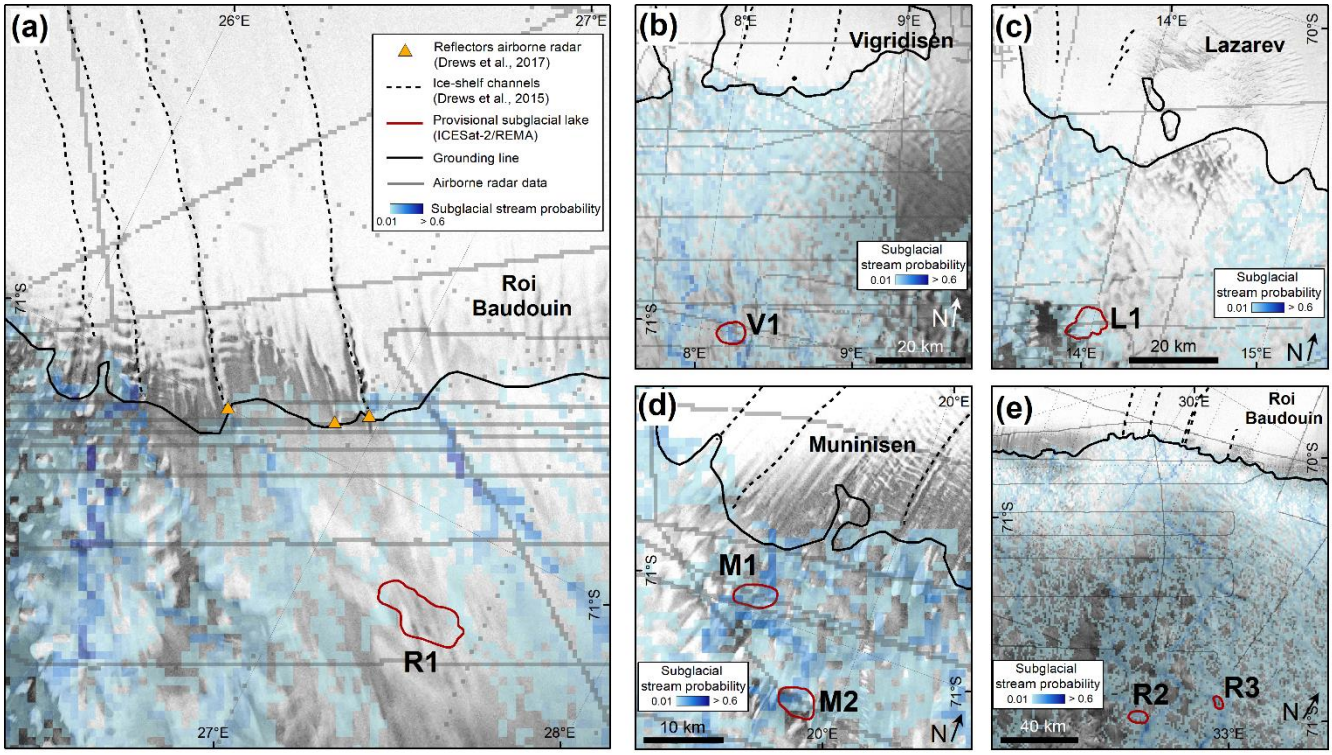

595 **Figure 6: Simulated subglacial water routing and mapped ice-shelf channels in the vicinity of identified active lake areas in this study (~~red~~ red outlines). Ice-shelf channels (black dashed lines) are from Drews (2015) (a-b) and manually delineated from REMA and RADARSAT imagery in this study (c-e). The ~~yellow~~ black solid line is the MEaSUREs grounding line (Rignot et al., 2016), the ~~purple~~ grey lines are radar data locations from Frémand et al. (2023), and the orange triangles are reflectors in airborne radar data interpreted as subglacial water flow outlets (Drews et al., 2017). The background image is the RADARSAT mosaic (Jezek et al.,**
600 **2013).**

605

Table 1: Subglacial lakes identified in this study. Lake areas are listed for those lakes where elevation anomalies were also derived from REMA strip differencing. Ice flow speed (Gardner et al., 2018), ice thickness (Fretwell et al., 2013; Morlighem et al., 2022) and bed elevation (Morlighem et al., 2022) are mean values within each inferred lake boundary. Bed elevation uncertainty is the median absolute deviation of 50 stochastic bed elevation simulations. Potential uUpstream catchment areas are ensemble-mean values ~~from~~ derived from water routing analyses using simulated bed. ~~the same topographic simulations.~~

Lake Name	Location/Distance from Grounding Line	Centre Lon, Lat (decimal degrees)	Area (km^2)	Ice flow speed ($m\ a^{-1}$)	Bedmap2 ice thickness (m)	BedMachine ice thickness (m)	Upstream catchment area (km^2)	Bed elevation (m above sea level)	Bed elevation uncertainty (m)
V1	Vigridisen (54 km)	8.19E, 70.99S	Unconfirmed	60	1247	1321	2.3×10^4	-552	58
L1	Lazarev (32 km)	13.97E, 70.67S	40.1	19	1020	1019	0.9×10^4	-558	47
M1	Muninisen (5 km)	19.60E, 70.98S	Unconfirmed	152	828	881	0.8×10^4	-724	28
M2	Muninisen (15 km)	19.87E, 71.07S	Unconfirmed	86	1008	924	1.2×10^4	-633	49
R1	Roi Baudouin (19 km)	27.41E, 71.10S	39.4	172	1137	1193	0.5×10^4	-737	76
R2	Roi Baudouin (115 km)	32.53E, 71.19S	21.5	17	1283	1391	1.4×10^4	-29	86
R3	Roi Baudouin (136 km)	31.65E, 71.44S	Unconfirmed	64	1503	1547	1.3×10^4	-162	97

Data Availability

ICESat-2 ATL11 Level 3B version 6 land ice height data are freely available from https://nsidc.org/data/atl11/versions/6. ICESat GLA12 version 34 land ice height data are freely available from https://nsidc.org/data/glah12/versions/34. Ice surface velocities from ITS-LIVE (Gardner et al., ~~2019~~2018) are available at https://its-live.jpl.nasa.gov/#data-portal. The REMA ice surface DEM strips (Howat et al., 2019) are available from the U.S. Polar Geospatial Center at https://www.pgc.umn.edu/data/rema/. The delineated lake boundaries are available as a shapefile from the Norwegian Polar Data Centre via https://doi.org/10.21334/npolar.2024.ab777130 and the predicted subglacial stream locations produced by our water routing analysis are available as a GeoTIFF from the Norwegian Polar Data Centre via https://doi.org/10.21334/npolar.2024.b438191c. ~~https://data.npolar.no/dataset/ 10.21334/npolar.2024.b438191c.~~

Code Availability

Code used to process and plot ICESat-2 ATL11 Level 3B version 6 land ice height data and ICESat GLAH12 version 34 land ice height data ~~are~~ is available at https://zenodo.org/records/13640820. The code and workflow for simulating the bed elevation grid ensemble and subglacial water flow routing is archived at~~:~~ https://zenodo.org/records/13627356.

Author Contributions

JA analysed the ICESat-2 and REMA data, performed the identification of active lakes, analysed the results and wrote the paper with input from all co-authors. CS and KM carried out stochastic bed topography simulations and the subglacial water flow routing analysis. GM contributed to the conception of the study and processed the ICESat data. All authors contributed to the discussion of the results and to editing of the manuscript.

Competing Interests

The contact author has declared that none of the authors have any competing interests.

Acknowledgements

JA and CS are funded by the Research Council of Norway's FRINATEK project (project number: 315246). JA is also funded by a national infrastructure grant from the Norwegian Space Agency to the Norwegian Polar Institute (contract number: 74CO2303). The bed elevation simulations were performed on resources provided by Sigma2 - the National Infrastructure for High-Performance Computing and Data Storage in Norway through project NN10061K.

References

Andersen, J.K., Rathmann, N., Hvidberg, C.S., Grinsted, A., Kusk, A., Merryman Boncori, J.P. and Mouginot, J.: Episodic subglacial drainage cascades below the Northeast Greenland Ice Stream. Geophys. Res. Lett., 50(12), https://doi.org/10.1029/2023GL103240, 2023.

Arthur, J.F., Stokes, C.R., Jamieson, S.S., Rachel Carr, J., Leeson, A.A. and Verjans, V.: Large interannual variability in supraglacial lakes around East Antarctica. Nat. Comm~~un~~., 13(1), 1711, https://doi.org/10.1038/s41467-022-29385-3, 2022.

Boening, C., Lebsock, M., Landerer, F. and Stephens, G.: Snowfall-driven mass change on the East Antarctic Ice Sheet. Geophys. Res. Lett., 39(21), https://doi.org/10.1029/2012GL053316, 2012.

Brenner, A.C., DiMarzio, J.P. and Zwally, H.J.: Precision and accuracy of satellite radar and laser altimeter data over the continental ice sheets. IEEE Trans. Geosci. Remote Sens., 45(2), 321-331, https://doi.org/10.1109/TGRS.2006.887172 2007.

Brunt, K.M., Smith, B.E., Sutterley, T.C:, Kurtz, N.T., Neumann, T.A.: Comparisons of Satellite and Airborne Altimetry With Ground-Based Data From the Interior of the Antarctic Ice Sheet. Geophys. Res. Lett., 48(2), e2020GL090572, https://doi.org/10.1029/2020GL090572, 2021.

Carter, S.P. and Fricker, H.A.: The supply of subglacial meltwater to the grounding line of the Siple Coast, West Antarctica. ~~Ann. Glaciol.,~~Ann. Glaciol., 53(60), 267-280, https://doi:10.3189/2012AoG60A119, 2012.

Carter, S.P., Fricker, H.A., Blankenship, D.D., Johnson, J.V., Lipscomb, W.H., Price, S.F. and Young, D.A.: Modeling 5 years of subglacial lake activity in the MacAyeal Ice Stream (Antarctica) catchment through assimilation of ICESat laser altimetry. J. Glaciol., 57(206), 1098-1112, https://doi:10.3189/002214311798843421, 2011.

Chartrand, A.M. and Howat, I.M.: Basal channel evolution on the Getz Ice Shelf, West Antarctica. J. Geophys. Res., 125(9), https://doi.org/10.1029/2019JF005293, 2020.

Chen, H., Rignot, E., Scheuchl, B. and Ehrenfeucht, S.: Grounding zone of Amery Ice Shelf, Antarctica, from differential synthetic-aperture radar interferometry. Geophys. Res. Lett., 50(6), https://doi.org/10.1029/2022GL102430, 2023.

Dell, R., Arnold, N., Willis, I., Banwell, A., Williamson, A., Pritchard, H. and Orr, A.: Lateral meltwater transfer across an Antarctic ice shelf. The Cryosphere, 14(7), 2313-2330, https://doi.org/10.5194/tc-14-2313-2020, 2020.

Dow, C.F., Ross, N., Jeofry, H., Siu, K. and Siegert, M.J.: Antarctic basal environment shaped by high-pressure flow through a subglacial river system. Nat. Geosci., 15(11), 892-898, https://doi.org/10.1038/s41561-022-01059-1, 2022.

Drews, R.: Evolution of ice-shelf channels in Antarctic ice shelves. The Cryosphere, 9, 1169–1181, https://doi.org/10.5194/tc-9-1169-2015, 2015.

Drews, R., Pattyn, F., Hewitt, I.J., Ng, F.S.L., Berger, S., Matsuoka, K., Helm, V., Bergeot, N., Favier, L. and Neckel, N.: Actively evolving subglacial conduits and eskers initiate ice shelf channels at an Antarctic grounding line. Nat. Comm~~un~~, 8(1), 15228, https://doi.org/10.1038/ncomms15228, 2017.

Drews, R., Schannwell, C., Ehlers, T.A., Gladstone, R., Pattyn, F. and Matsuoka, K.: Atmospheric and oceanographic signatures in the ice shelf channel morphology of Roi Baudouin Ice Shelf, East Antarctica, inferred from radar data. J. Geophys. Res., 125(7), https://doi.org/10.1029/2020JF005587, 2020.

Dunmire, D., Lenaerts, J.T.M., Banwell, A.F., Wever, N., Shragge, J., Lhermitte, S., Drews, R., Pattyn, F., Hansen, J.S.S., Willis, I.C. and Miller, J.: Observations of buried lake drainage on the Antarctic Ice Sheet. Geophys. Res. Lett., 47(15), https://doi.org/10.1029/2020GL087970, 2020.

~~ESA.: Sentinel-1: ESA's Radar Observatory Mission for GMES Operational Services. ESA SP-1322/1, ISBN 978-92-9221-418-0, 2012.~~

Fan, Y.; Hao, W.; Zhang, B.; Ma, C.; Gao, S.; Shen, X.; Li, F.: Monitoring the Hydrological Activities of Antarctic Subglacial Lakes Using CryoSat-2 and ICESat-2 Altimetry Data. Remote Sens. 14, 898, https://doi.org/10.3390/rs14040898, 2022.

Fan, Y., Ke, C.Q., Shen, X., Xiao, Y., Livingstone, S.J. and Sole, A.J.: Subglacial lake activity beneath the ablation zone of the Greenland Ice Sheet. The Cryosphere, 17(4), 1775-1786, https://doi.org/10.5194/tc-17-1775-2023, 2023.

Flament, T., Berthier, E. and Rémy, F.: Cascading water underneath Wilkes Land, East Antarctic ice sheet, observed using altimetry and digital elevation models. The Cryosphere, 8(2), 673-687, https://doi.org/10.5194/tc-8-673-2014, 2014.

Frémand, A.C., Fretwell, P., Bodart, J.A., Pritchard, H.D., Aitken, A., Bamber, J.L., Bell, R., Bianchi, C., Bingham, R.G., Blankenship, D.D. and Casassa, G.: Antarctic Bedmap data: Findable, Accessible, Interoperable, and Reusable (FAIR) sharing of 60 years of ice bed, surface, and thickness data. Earth Syst. Sci. Data, 15(7), https://doi.org/10.5194/essd-15-2695-2023, 2023.

Fricker, H.A. and Padman, L.: Ice shelf grounding zone structure from ICESat laser altimetry. Geophys. Res. Lett., 33(15), https://doi.org/10.1029/2006GL026907, 2006.

Fricker, H.A., Scambos, T., Bindschadler, R., and Padman, L.: An Active Subglacial Water System in West Antarctica Mapped from Space. Science, 315(5818): 1544-1548, https://doi.org/10.1126/science.1136897, 2007.

Fricker, H.A. and Scambos, T.: Connected subglacial lake activity on lower Mercer and Whillans ice streams, West Antarctica, 2003–2008. J. Glaciol., 55(190), 303-315, https://doi.org/10.3189/002214309788608813, 2009.

Fricker, H.A., Scambos, T., Carter, S., Davis, C., Haran, T. and Joughin, I.: Synthesizing multiple remote-sensing techniques for subglacial hydrologic mapping: application to a lake system beneath MacAyeal Ice Stream, West Antarctica. J. Glaciol., 56(196), 187-199, https://doi.org/10.3189/002214310791968557, 2010.

Fricker HA, Carter SP, Bell RE, Scambos T.: Active lakes of Recovery Ice Stream, East Antarctica: a bedrock-controlled subglacial hydrological system. J. Glaciol., 60(223), 1015-1030, https://doi.org/10.3189/2014JoG14J063, 2014.

Gardner, A. S., G. Moholdt, T. Scambos, M. Fahnstock, S. Ligtenberg, M. van den Broeke, and J. Nilsson: Increased West Antarctic and unchanged East Antarctic ice discharge over the last 7 years, The Cryosphere, 12(2): 521–547, https://doi.org/10.5194/tc-12-521-2018, 2018.

Goel, V., Martín, C., Matsuoka, K.: Evolution of ice rises in the Fimbul Ice Shelf, Dronning Maud Land, over the last millennium. Ant. Sci., 36(2), 2024, https://doi:10.1017/S0954102023000330.

Goeller, S., Steinhage, D., Thoma, M. and Grosfeld, K.: Assessing the subglacial lake coverage of Antarctica. Ann. Glaciol., 57(72), 109-117, https://doi.org/10.1017/aog.2016.23, 2016.

Goldberg, D., Twelves, A., Holland, P., Wearing, M.G.: The Non-Local Impacts of Antarctic Subglacial Runoff. JGR Oceans 128(10) https://doi.org/10.1029/2023JC019823, 2023.

~~Gong, F., Zhang, K. and Liu, S.: Retrieving the grounding lines of the Riiser-Larsen Ice Shelf using Sentinel-1 SAR images. Int. J. Digit. Earth, 16(1), 2467-2486, https://doi.org/10.1080/17538947.2023.2229785, 2023.~~

Gray, L., Joughin, I., Tulaczyk, S., Spikes, V.B., Bindschadler, R. and Jezek, K.: Evidence for subglacial water transport in the West Antarctic Ice Sheet through three-dimensional satellite radar interferometry. Geophys. Res. Lett., 32(3), https://doi.org/10.1029/2004GL021387, 2005.

Gwyther, D.E., Dow, C.F., Jendersie, S., Gourmelen, N. and Galton-Fenzi, B.K.: Subglacial freshwater drainage increases simulated basal melt of the Totten Ice Shelf. Geophys. Res. Lett., 50(12), https://doi.org/10.1029/2023GL103765, 2023.

Hayden, A., & Dow, C.: Examining the effect of ice dynamic changes on subglacial hydrology through modelling of a synthetic Antarctic glacier. J. Glaciol., 1-14. https://doi.org/10.1017/jog.2023.65, 2023.

Hodgson, D.A., Jordan, T.A., Ross, N., Riley, T.R. and Fretwell, P.T.: Drainage and refill of an Antarctic Peninsula subglacial lake reveal an active subglacial hydrological network. The Cryosphere, 16(12), 4797-4809, https://doi.org/10.5194/tc-16-4797-2022, 2022.

Hoffman, A.O., Christianson, K., Shapero, D., Smith, B.E. and Joughin, I.: Brief communication: Heterogenous thinning and subglacial lake activity on Thwaites Glacier, West Antarctica. The Cryosphere, 14(12), 4603-4609, https://doi.org/10.5194/tc-14-4603-2020, 2020.

Hogg, A., Shepherd, A., Gourmelen, N., & Engdhal, M.: Grounding line migration from 1992 to 2011 on Petermann Glacier, North West Greenland. J. Glaciol., 62(236), 1104-1114, https://doi.org/10.1017/jog.2016.83, 2016.

Howat, I.M., Porter, C., Smith, B.E., Noh, M.J. and Morin, P.: The reference elevation model of Antarctica. The Cryosphere, 13(2), 665-674, https://doi.org/10.5194/tc-13-665-2019, 2019.

Humbert, A., Steinhage, D., Helm, V., Beyer, S. and Kleiner, T.: Missing evidence of widespread subglacial lakes at Recovery Glacier, Antarctica. J. Geophys. Res., 123(11), 2802-2826, https://doi.org/10.1029/2017JF004591, 2018.

Jenkins, A.: Convection-driven melting near the grounding lines of ice shelves and tidewater glaciers. JPO, 41(12), 2279-2294, https://doi.org/10.1175/JPO-D-11-03.1, 2011.

Jezek, K. C., Curlander, J. C., Carsey, F., Wales, C., and Barry, R.G.: RAMP AMM-1 SAR Image Mosaic of Antarctica, Version2. Boulder, Colorado USA, NSIDC: National Snow and Ice Data Center, https://doi.org/10.5067/8AF4ZRPULS4H, 2013.

Kim, B.H., Lee, C.K., Seo, K.W., Lee, W.S. and Scambos, T.: Active subglacial lakes and channelized water flow beneath the Kamb Ice Stream. The Cryosphere, 10(6), 2971-2980, https://doi.org/10.5194/tc-10-2971-2016, 2016.

Kohler, J., Neumann, T.A., Robbins, J.W., Tronstad, S. and Melland, G.: ICESat elevations in Antarctica along the 2007–09 Norway–USA traverse: Validation with ground-based GPS. IEEE GRSL, 51(3), 1578-1587, https://doi.org/10.1109/TGRS.2012.2207963, 2012.

Le Brocq, A.M., Ross, N., Griggs, J.A., Bingham, R.G., Corr, H.F., Ferraccioli, F., Jenkins, A., Jordan, T.A., Payne, A.J., Rippin, D.M. and Siegert, M.J.: Evidence from ice shelves for channelized meltwater flow beneath the Antarctic Ice Sheet. Nat. Geosci, 6(11), 945-948, https://doi.org/10.1038/ngeo1977, 2013.

Lepp, A.P., Simkins, L.M., Anderson, J.B., Clark, R.W., Wellner, J.S., Hillenbrand, C.D., Smith, J.A., Lehrmann, A.A., Totten, R., Larter, R.D. and Hogan, K.A.: Sedimentary signatures of persistent subglacial meltwater drainage from Thwaites Glacier, Antarctica. Front. Earth Sci., 10, https://doi.org/10.3389/feart.2022.863200, 2022.

Liang, D., Guo, H., Zhang, L., Li, H. and Wang, X.: Sentinel-1 EW mode dataset for Antarctica from 2014–2020 produced by the CASEarth Cloud Service Platform. Big Earth Data, 6(4), 385-400, https://doi.org/10.1080/20964471.2021.1976706, 2022. Li, Y., Lu, Y. and Siegert, M.J.: Radar sounding confirms a

hydrologically active deep-water subglacial lake in East Antarctica. Front. Earth Sci., 8, https://doi.org/10.3389/feart.2020.00294, 2020.

Li, L., Aitken, A.R., Lindsay, M.D. and Kulessa, B.: Sedimentary basins reduce stability of Antarctic ice streams through groundwater feedbacks. Nature Geoscience, 15(8), 645-650, https://doi.org/10.1038/s41561-022-00992-5, 2022.

Livingstone, S.J., Li, Y., Rutishauser, A., Sanderson, R.J., Winter, K., Mikucki, J.A., Björnsson, H., Bowling, J.S., Chu, W., Dow, C.F. and Fricker, H.A.: Subglacial lakes and their changing role in a warming climate. Nat. Rev. Earth Environ., 3(2), 106-124, https://doi.org/10.1038/s43017-021-00246-9, 2022.

MacKie, E.J., Schroeder, D.M., Caers, J., Siegfried, M.R. and Scheidt, C.: Antarctic topographic realizations and geostatistical modeling used to map subglacial lakes. J. Geophys. Res. Earth Surf., 125(3), https://doi.org/10.1029/2019JF005420, 2020.

MacKie, E.J., Schroeder, D.M., Zuo, C., Yin, Z. and Caers, J.: Stochastic modeling of subglacial topography exposes uncertainty in water routing at Jakobshavn Glacier. J. Glaciol., 67(261), https://doi.org/10.1017/jog.2020.84, 2021.

MacKie, E. J., Field, M., Wang, L., Yin, Z., Schoedl, N., Hibbs, M., & Zhang, A.: GStatSim V1.0: A Python package for geostatistical interpolation and conditional simulation. GMD, 16(13), 3765–3783, https://doi.org/10.5194/gmd-16-3765-2023, 2023.

Mahagaonkar A., Moholdt G., Glaude Q., Schuler T.V.: Supraglacial lake evolution and its drivers in Dronning Maud Land, East Antarctica. J. Glaciol., 1-15. https://doi.org/10.1017/jog.2024.66, 2024. ~~Mahagaonkar, A., Moholdt, G.: Surface meltwater lake extents and depths for 5 ice shelves of DML, East Antarctica, 2014-2021 [Data set]. Norwegian Polar Institute. https://doi.org/10.21334/npolar.2023.31aae21f, 2022.~~

Malczyk, G., Gourmelen, N., Goldberg, D., Wuite, J. and Nagler, T.: Repeat subglacial lake drainage and filling beneath Thwaites Glacier. Geophys. Res. Lett., 47(23), https://doi.org/10.1029/2020GL089658, 2020.

Malczyk G, Gourmelen N, Werder M, Wearing M, Goldberg D.: Constraints on subglacial melt fluxes from observations of active subglacial lake recharge. J. Glaciol., 1-15, https://doi.org/10.1017/jog.2023.70, 2023.

Markus, T., Neumann, T., Martino, A., Abdalati, W., Brunt, K., Csatho, B., Farrell, S., Fricker, H., Gardner, A., Harding, D. and Jasinski, M.: The Ice, Cloud, and land Elevation Satellite-2 (ICESat-2): science requirements, concept, and implementation. Remote Sens. Environ., 190, 260-273, https://doi.org/10.1016/j.rse.2016.12.029, 2017.

Matsuoka, K., Forsberg, R., Ferraccioli, F., Moholdt, G., and Morlighem, M.: Circling Antarctica to unveil the bed below its icy edge, Eos, 103, https://doi.org/10.1029/2022EO220276, 2022.

Mälicke, M.: SciKit-GStat 1.0: a SciPy-flavored geostatistical variogram estimation toolbox written in Python. Geosci. Model Dev., 15(6), 2505-2532, https://doi.org/10.5194/gmd-15-2505-2022, 2022.

Medley, B., Lenaerts, J.T.M., Dattler, M., Keenan, E. and Wever, N.: Predicting Antarctic net snow accumulation at the kilometer scale and its impact on observed height changes. Geophys. Res. Lett., 49(20), https://doi.org/10.1029/2022GL099330, 2022.

Miles, B.W., Stokes, C.R., Jamieson, S.S., Jordan, J.R., Gudmundsson, G.H. and Jenkins, A.: High spatial and temporal variability in Antarctic ice discharge linked to ice shelf buttressing and bed geometry. Sci. Rep., 12(1), 10968, https://doi.org/10.1038/s41598-022-13517-2, 2022.

Moholdt, G., Nuth, C., Hagen, J.O., Kohler, J.: Recent elevation changes of Svalbard glaciers derived from ICESat laser altimetry. Remote Sens. Environ. 114(11), 2756-2767, https://doi.org/10.1016/j.rse.2010.06.008, 2010.

Moon, J., Lee, H. and Lee, H.: Elevation Change of CookE2 Subglacial Lake in East Antarctica Observed by DInSAR and Time-Segmented PSInSAR. Remote Sens., 14(18), 4616, https://doi.org/10.3390/rs14184616, 2022.

Morlighem, M.: MEaSUREs BedMachine Antarctica, Version 3. Boulder, Colorado USA. NASA National Snow and Ice Data Center Distributed Active Archive Center. Date Accessed 11-22-2023, https://doi.org/10.5067/FPSU0V1MWUB6, 2022.

Mouginot, J., B. Scheuchl, and E. Rignot.: 2017. MEaSURE's Antarctic Boundaries for IPY 2007-2009 from Satellite Radar, Version 2. Boulder, Colorado USA. NASA National Snow and Ice Data Center Distributed Active Archive Center., doi: http://dx.doi.org/10.5067/AXE4121732AD, 2017..

Neckel, N., Franke, S., Helm, V., Drews, R. and Jansen, D.; Evidence of Cascading Subglacial Water Flow at Jutulstraumen Glacier (Antarctica) Derived From Sentinel-1 and ICESat-2 Measurements. Geophys. Res. Lett., 48(20), https://doi.org/10.1029/2021GL094472, 2021.

Nilsson, J., Gardner, A. S., and Paolo, F. S.: Elevation change of the Antarctic Ice Sheet: 1985 to 2020, Earth Syst. Sci. Data, 14, 3573–3598, https://doi.org/10.3189/002214308784886171, 2022.

Pattyn, F.: Investigating the stability of subglacial lakes with a full Stokes ice-sheet model. J. Glaciol, 54(185), 353-361, 2008.

Pattyn, F.: Antarctic subglacial conditions inferred from a hybrid ice sheet/ice stream model. EPSL 295(3-4), 451-461, https://doi.org/10.1016/j.epsl.2010.04.025, 2010.

Pattyn, F., Carter, S.P. and Thoma, M.: Advances in modelling subglacial lakes and their interaction with the Antarctic ice sheet. Philos Trans A Math Phys Eng Sci, 374(2059), https://doi.org/10.1098/rsta.2014.0296, 2016.

Pratap, B., Dey, R., Matsuoka, K., Moholdt, G., Lindbäck, K., Goel, V., Laluraj, L., Thamban, M.: Three-decade spatial patterns in surface mass balance of the Nivlisen Ice Shelf, central Dronning Maud Land, East Antarctica. J. Glac., 68(267), https://doi:10.1017/jog.2021.93, 2022.

Priergaard Zinck, A., Wouters, B., Lambert, E., Lhermitte, S.; Unveiling spatial variability within the Dotson Melt Channel through high-resolution basal melt rates from the Reference Elevation Model of Antarctica. The Cryosphere 17(9) 3785-3801, https://doi.org/10.5194/tc-17-3785-2023, 2023.

Rignot, E., Mouginot, J., and Scheuchl, B.: MEaSUREs Antarctic Grounding Line from Differential Satellite Radar Interferometry, Version 2. Boulder, Colorado USA. NASA National Snow and Ice Data Center Distributed Active Archive Center. https://doi.org/10.5067/IKBWW4RYHF1Q, 2016.

Robel, A.A., Wilson, E. and Seroussi, H.: Layered seawater intrusion and melt under grounded ice. The Cryosphere, 16(2), 451-469, https://doi.org/10.5194/tc-16-451-2022, 2022.

Scambos, T.A, Berthier, E., Shuman, C.A.: The triggering of subglacial lake drainage during rapid glacier drawdown: Crane Glacier, Antarctic Peninsula. Ann. Glaciol. 52(59), 74-82, https://doi.org/10.3189/172756411799096204, 2011.

~~Schodlok, M.P., Menemenlis, D. and Rignot, E.J.: Ice shelf basal melt rates around Antarctica from simulations and observations. J. Geophys. Res. Oceans, 121(2), 1085-1109, https://doi.org/10.1002/2015JC011117, 2016.~~

Schutz, B.E., Zwally, H.J., Shuman, C.A., Hancock, D. and DiMarzio, J.P.: Overview of the ICESat mission. Geophysical research letters, 32(21), https://doi:10.1029/2005GL024009, 2005.

Sergienko, O.V., MacAyeal, D.R. and Bindschadler, R.A.: Causes of sudden, short-term changes in ice-stream surface elevation. Geophys. Res. Lett., 34(22), https://doi.org/10.1029/2007GL031775, 2007.

Shackleton, C., Matsuoka, K., Moholdt, G., Van Liefferinge, B. and Paden, J.: Stochastic simulations of bed topography constrain geothermal heat flow and subglacial drainage near Dome Fuji, East Antarctica. J. Geophys. Res., 128(11), https://doi.org/10.1029/2023JF007269, 2023.

Shean, D.E., Joughin, I.R., Dutrieux, P., Smith, B.E. and Berthier, E.: Ice shelf basal melt rates from a high-resolution digital elevation model (DEM) record for Pine Island Glacier, Antarctica. The Cryosphere, 13(10), 2633-2656, https://doi.org/10.5194/tc-13-2633-2019, 2019.

Shreve, R.L.: Movement of water in glaciers. J. Glaciol., 11(62), 205-214, https://doi.org/10.3189/S002214300002219X, 1972.

Siegfried, M., Fricker, H.A., Carter, S.P., Tulaczyk, T.: Episodic ice velocity fluctuations triggered by a subglacial flood in West Antarctica. Geophys. Res. Lett., 43(6), 2640-2648, https://doi.org/10.1002/2016GL067758, 2016.

Siegfried, M.R. and Fricker, H.A.: Thirteen years of subglacial lake activity in Antarctica from multi-mission satellite altimetry. Ann. Glaciol., 59(76pt1), 42-55, https://doi.org/10.1017/aog.2017.36, 2018.

Siegfried, M.R. and Fricker, H.A.: Illuminating active subglacial lake processes with ICESat-2 laser altimetry. Geophys. Res. Lett., 48(14), https://doi.org/10.1029/2020GL091089, 2021.

Smith, B.E., Fricker, H.A., Joughin, I.R., and Tulaczyk, S.: An inventory of active subglacial lakes in Antarctica detected by ICESat (2003-2008). J. Glac., 2009. 55(192), 573-595, https://doi.org/10.3189/002214309789470879, 2009.

Smith, B.E., Gourmelen, N., Huth, A. and Joughin, I.: Connected subglacial lake drainage beneath Thwaites glacier, west Antarctica. The Cryosphere, 11(1), 451-467, https://doi.org/10.5194/tc-11-451-2017, 2017.

Smith, B.E, Fricker, H.A., Gardner, A.S., Medley, B., Nilsson, J., Paolo, F.S., Holschuh, N., Adusumilli, S., Brunt, K., Csatho, B. and Harbeck, K.: Pervasive ice sheet mass loss reflects competing ocean and atmosphere processes. Science, 368(6496), 1239-1242, https://doi.org/10.1126/science.aaz5845, 2020.

Smith, B.E, Dickinson, S., Jelley, B. P., Neumann, T. A., Hancock, D., Lee, J. & Harbeck, K.: ATLAS/ICESat-2 L3B Slope-Corrected Land Ice Height Time Series. (ATL11, Version 6). Boulder, Colorado USA. NASA National Snow and Ice Data Center Distributed Active Archive Center. Date Accessed 11-01-2023, https://doi.org/10.5067/ATLAS/ATL11.006, 2023a.

Smith, B.E., Medley, B., Fettweis, X., Sutterley, T., Alexander, P., Porter, D. and Tedesco, M.: Evaluating Greenland surface-mass-balance and firn-densification data using ICESat-2 altimetry. The Cryosphere, 17(2), 789-808, https://doi.org/10.5194/tc-17-789-2023, 2023b.

Stearns, L.A., Smith, B.E., and Hamilton, G.S.: Increased flow speed on a large East Antarctic outlet glacier caused by subglacial floods. Nat. Geosci, 2008. 1(12): 827-831, https://doi.org/10.1038/ngeo356, 2008.

Tarboton, D.G.: A new method for the determination of flow directions and upslope areas in grid digital elevation models. Water Resour. Res., 33(2), 309-319, https://doi.org/10.1029/96WR03137, 1997.

~~Trusel, L.D., Frey, K.E., Das, S.B., Munneke, P.K. and Van Den Broeke, M.R.: Satellite-based estimates of Antarctic surface meltwater fluxes. Geophys. Res. Lett., 40(23), 6148-6153, https://doi.org/10.1002/2013GL058138, 2013.~~

Wadham, J.L., De'ath, R., Monteiro, F.M., Tranter, M., Ridgwell, A., Raiswell, R. and Tulaczyk, S.: The potential role of the Antarctic Ice Sheet in global biogeochemical cycles. Earth Environ. Sci. Trans., 104(1), 55-67, https://doi.org/10.1017/S1755691013000108, 2013.

Whiteford, A., Horgan, H.J., Leong, W.J. and Forbes, M.: Melting and refreezing in an ice shelf basal channel at the grounding line of the Kamb Ice Stream, West Antarctica. J. Geophys. Res., 127(11), https://doi.org/10.1029/2021JF006532, 2022.

Wright, A., & Siegert, M.: A fourth inventory of Antarctic subglacial lakes. Ant. Sci. 24(6), 659-664. https://doi.org/10.1017/S095410201200048X, 2012.

~~Zwally, H. J., Schutz, B., Abdalati, W., Abshire, J., Bentley, C., Brenner, A., Bufton, J., Dezio, J., Hancock, D., Harding, D., Herring, T., Minster, B., Quinn, K., Palm, S., Spinhirne, J., and Thomas, R.: ICESat's laser measurements of polar ice, atmosphere, ocean, and land, J. Geodyn., 34, 405–445, https://doi.org/10.1016/S0264-3707(02)00042-X, 2002.~~

Supplementary Information

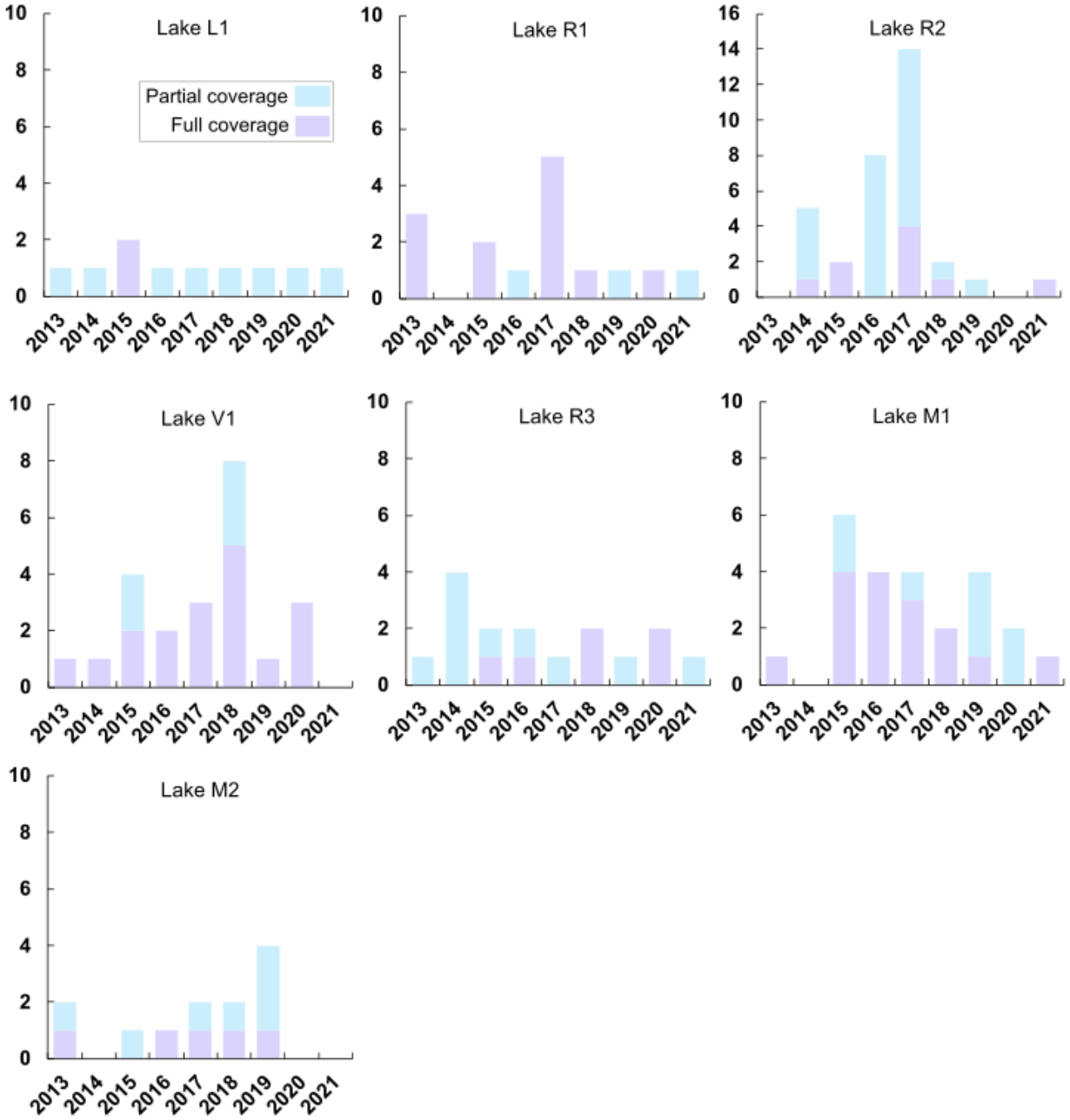

Supplementary Figure 1: Availability of time-stamped 2-m REMA strips over lakes identified from satellite altimetry, coloured according to partial coverage (blue) or full coverage (purple) of each lake.

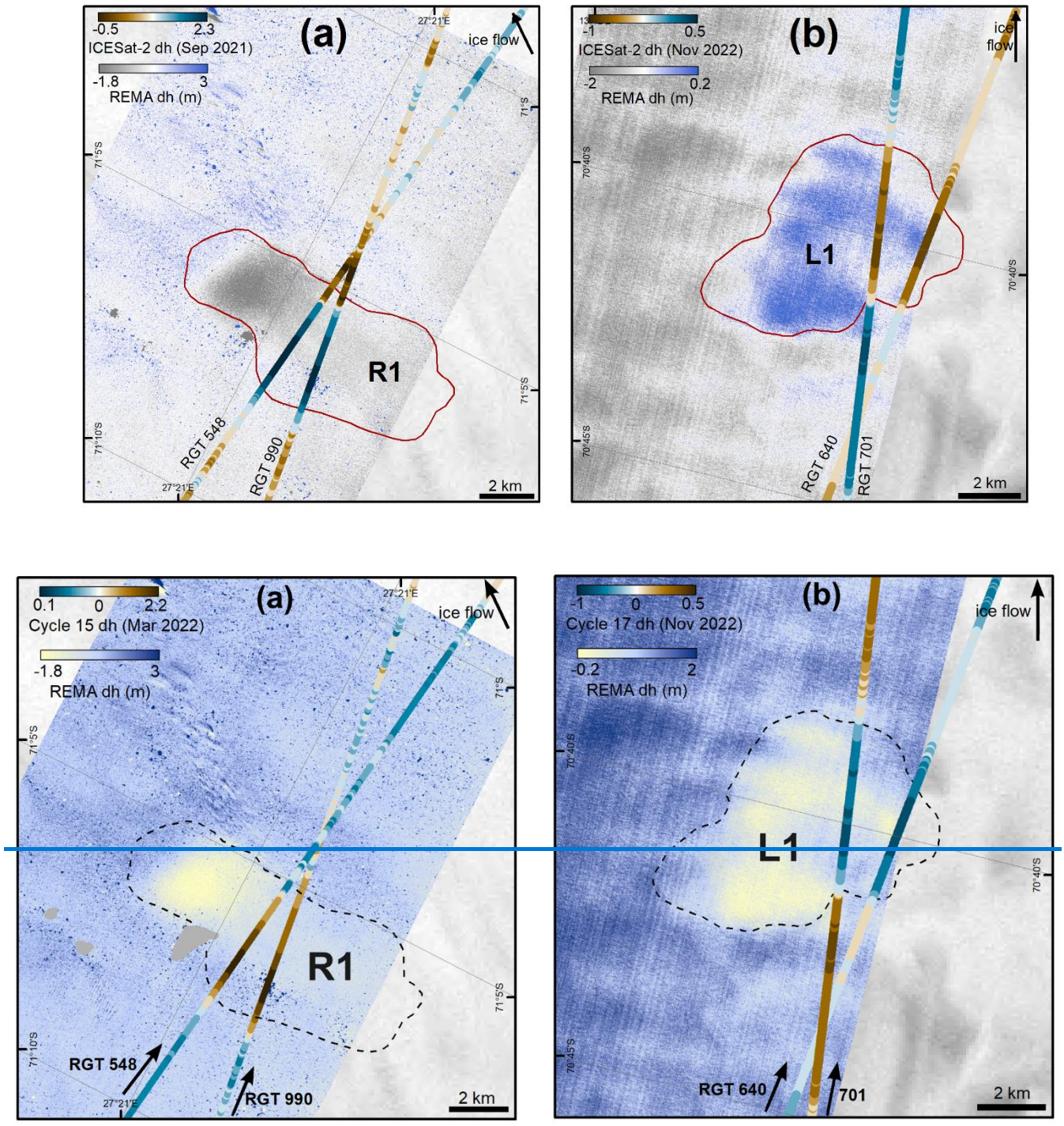

Supplementary Fig. 2: Ice surface elevation change from REMA strip differencing for Lakes R1 (a) and L1 (b). Regions of ice surface subsidence (yellow shading) between time-stamped REMA strip pairs (7th December 2016 – 21st December 2017 and 12th September 2015 – 10th December 2016) are delineated by the dashed lines. Each example highlights the spatial cooccurrence between localised

ice surface subsidence and surface elevation anomalies along the intersecting ICESat-2 tracks, suggesting Lakes R1 and L1 were draining during the period bounded by the REMA strip pairs.

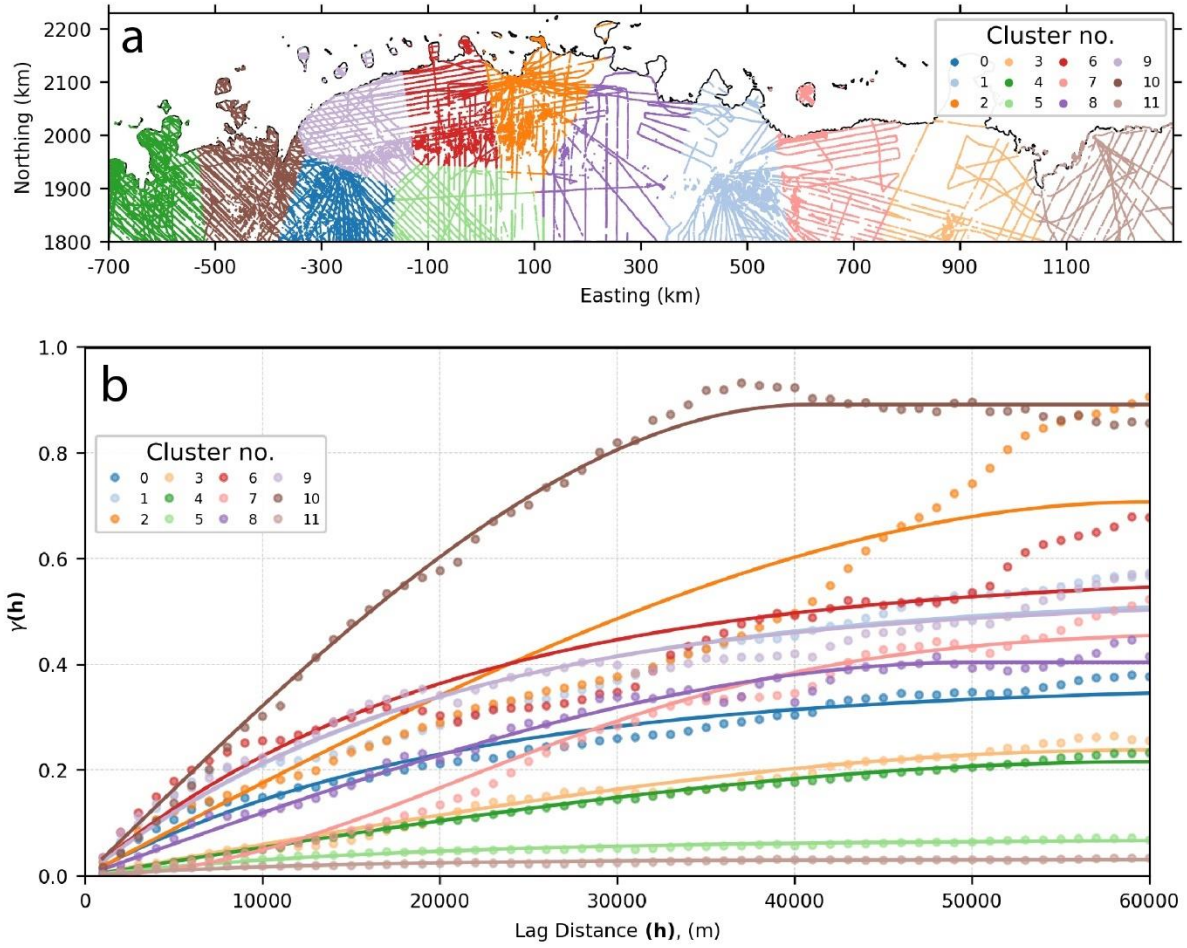

Supplementary Figure 3: Clustered bed elevation data and associated variograms. a) Map showing ~~the~~radar-survey derived bed elevation data ~~- data~~ divided into 12 regional clusters using a k-means clustering algorithm on measurement coordinates. Map is in a polar stereographic projection with true scale latitude of -71 and central longitude of 10 degrees. b) ~~, with associated variograms plotted below.~~ Experimental variogram (points) and modelled variogram (curves) are shown for normalised bed elevations in each of the 12 regions. The best-fitting model types are either exponential (clusters 0,5,6,9,11), spherical (clusters 1,2,3,4,8,10) ~~and~~or Gaussian (cluster 7).

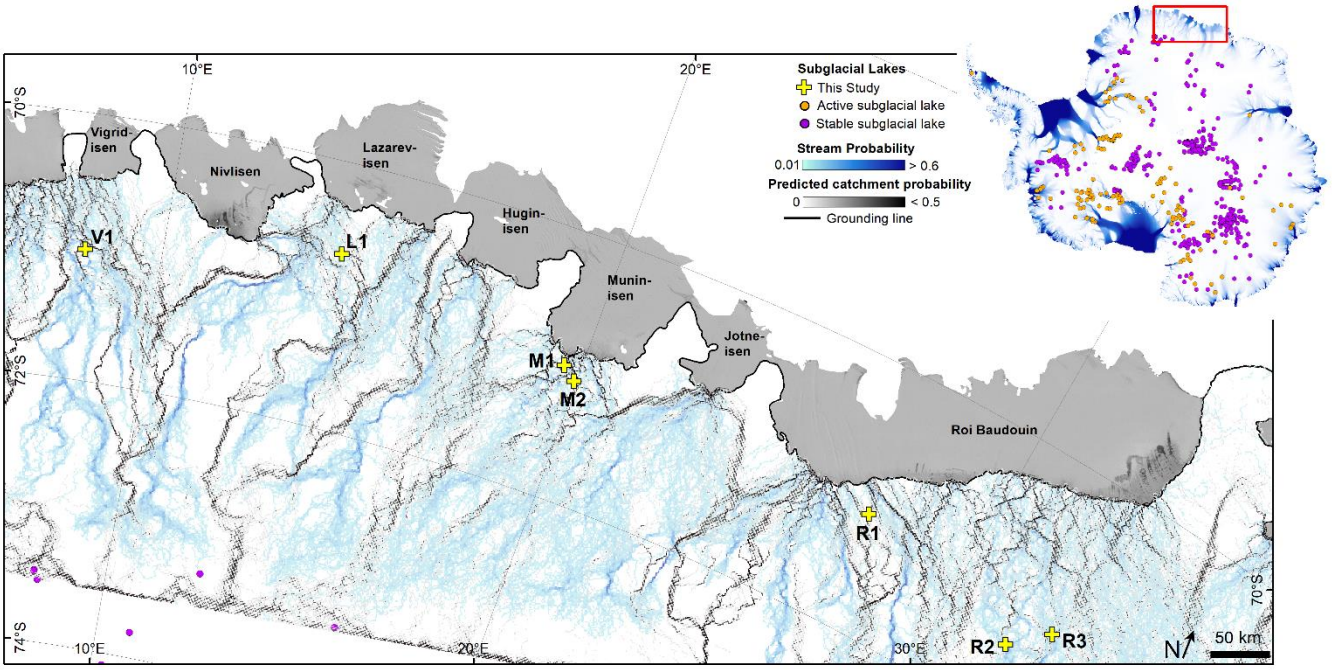

Supplementary Figure 4: Probability of subglacial drainage catchment boundaries derived from water routing analyses over the ensemble of 50 stochastic bed simulations. The dashed black line is the MEaSUREs grounding line (Rignot et al., 2016) and ice-shelf imagery is from the MODIS mosaic (Haran et al., 2021). Subglacial lake locations depicted in the inset map are from Livingstone et al. (2022), where active lakes are represented by orange dots and stable lakes by green dots. Simulations of subglacial water drainage pathways are limited to ca. <73°.

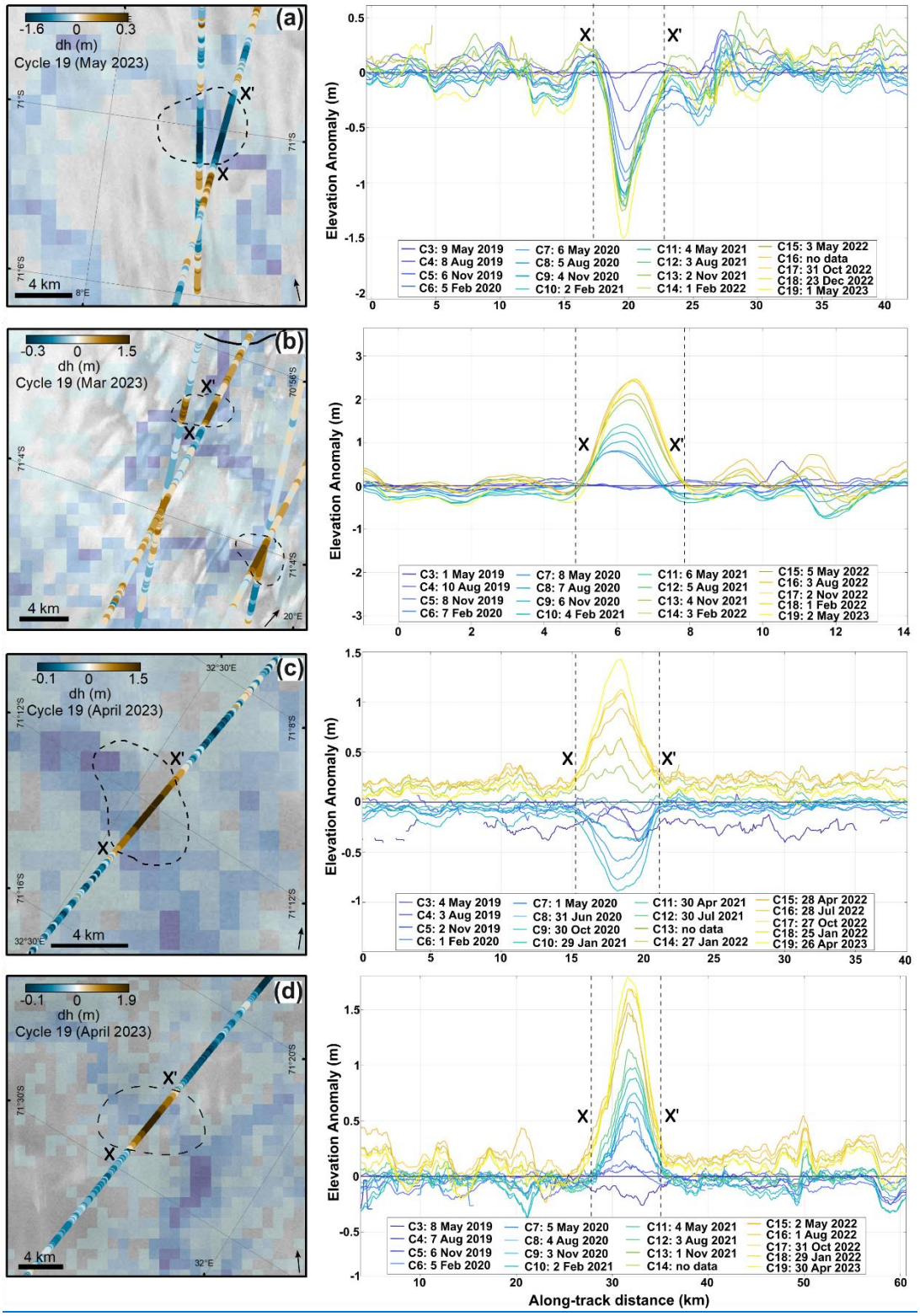
(a)
-1.6 0 0.3
dh (m)
Cycle 19 (May 2023)
X
X'
71°S
71°6'S
4 km
8°E
Elevation Anomaly (m)
C3: 9 May 2019
C4: 8 Aug 2019
C5: 6 Nov 2019
C6: 5 Feb 2020
C7: 6 May 2020
C8: 5 Aug 2020
C9: 4 Nov 2020
C10: 2 Feb 2021
C11: 4 May 2021
C12: 3 Aug 2021
C13: 2 Nov 2021
C14: 1 Feb 2022
C15: 3 May 2022
C16: no data
C17: 31 Oct 2022
C18: 23 Dec 2022
C19: 1 May 2023
(b)
-0.3 0 1.5
dh (m)
Cycle 19 (Mar 2023)
70°58'S
71°4'S
20°E
C3: 1 May 2019
C4: 10 Aug 2019
C5: 8 Nov 2019
C6: 7 Feb 2020
C7: 8 May 2020
C8: 7 Aug 2020
C9: 6 Nov 2020
C10: 4 Feb 2021
C11: 6 May 2021
C12: 5 Aug 2021
C13: 4 Nov 2021
C14: 3 Feb 2022
C15: 5 May 2022
C16: 3 Aug 2022
C17: 2 Nov 2022
C18: 1 Feb 2022
C19: 2 May 2023
(c)
-0.1 0 1.5
dh (m)
Cycle 19 (April 2023)
32°30'E
71°12'S
71°18'S
C3: 4 May 2019
C4: 3 Aug 2019
C5: 2 Nov 2019
C6: 1 Feb 2020
C7: 1 May 2020
C8: 31 Jun 2020
C9: 30 Oct 2020
C10: 29 Jan 2021
C11: 30 Apr 2021
C12: 30 Jul 2021
C13: no data
C14: 27 Jan 2022
C15: 28 Apr 2022
C16: 28 Jul 2022
C17: 27 Oct 2022
C18: 25 Jan 2022
C19: 26 Apr 2023
(d)
-0.1 0 1.9
dh (m)
Cycle 19 (April 2023)
71°20'S
71°30'S
32°E
C3: 8 May 2019
C4: 7 Aug 2019
C5: 6 Nov 2019
C6: 5 Feb 2020
C7: 5 May 2020
C8: 4 Aug 2020
C9: 3 Nov 2020
C10: 2 Feb 2021
C11: 4 May 2021
C12: 3 Aug 2021
C13: 1 Nov 2021
C14: no data
C15: 2 May 2022
C16: 1 Aug 2022
C17: 31 Oct 2022
C18: 29 Jan 2022
C19: 30 Apr 2023
Along-track distance (km)

Supplementary Figure 5~~6~~: Ice surface elevation displacements for Lakes V1, M1, M2, R2 and R3 derived from ICESat-2. Transects X-X' in each panel highlight significant (>1 m) ice surface elevation anomalies along ICESat-2 tracks. Graphs show along-track ice surface elevation displacements relative to ICESat-2 Cycle 3 (April/May 2019). Colours correspond to individual ICESat-2 cycles.

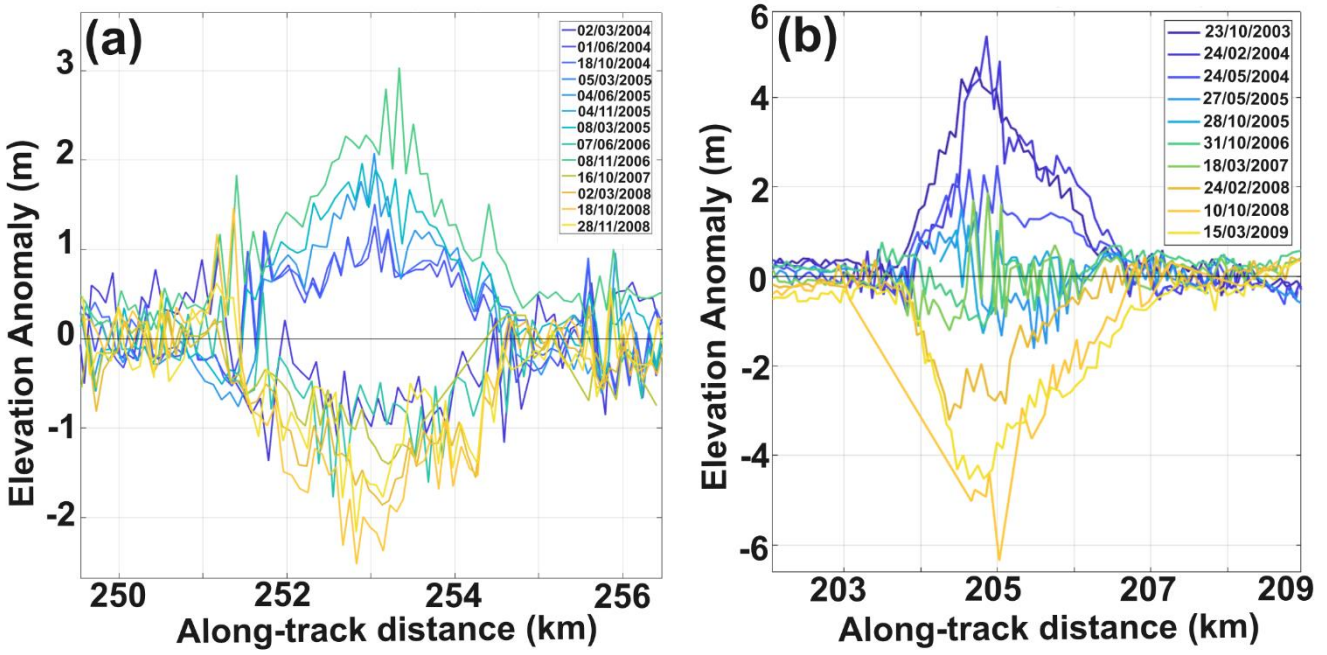

Supplementary Figure 6~~7~~: Ice surface elevation displacement anomalies from two ICESat tracks over Lake R1 (a, Track 21) and Lake L1 (b, Track 134). Elevation anomalies are calculated with respect to surface plane fits representing averaged surface elevation.

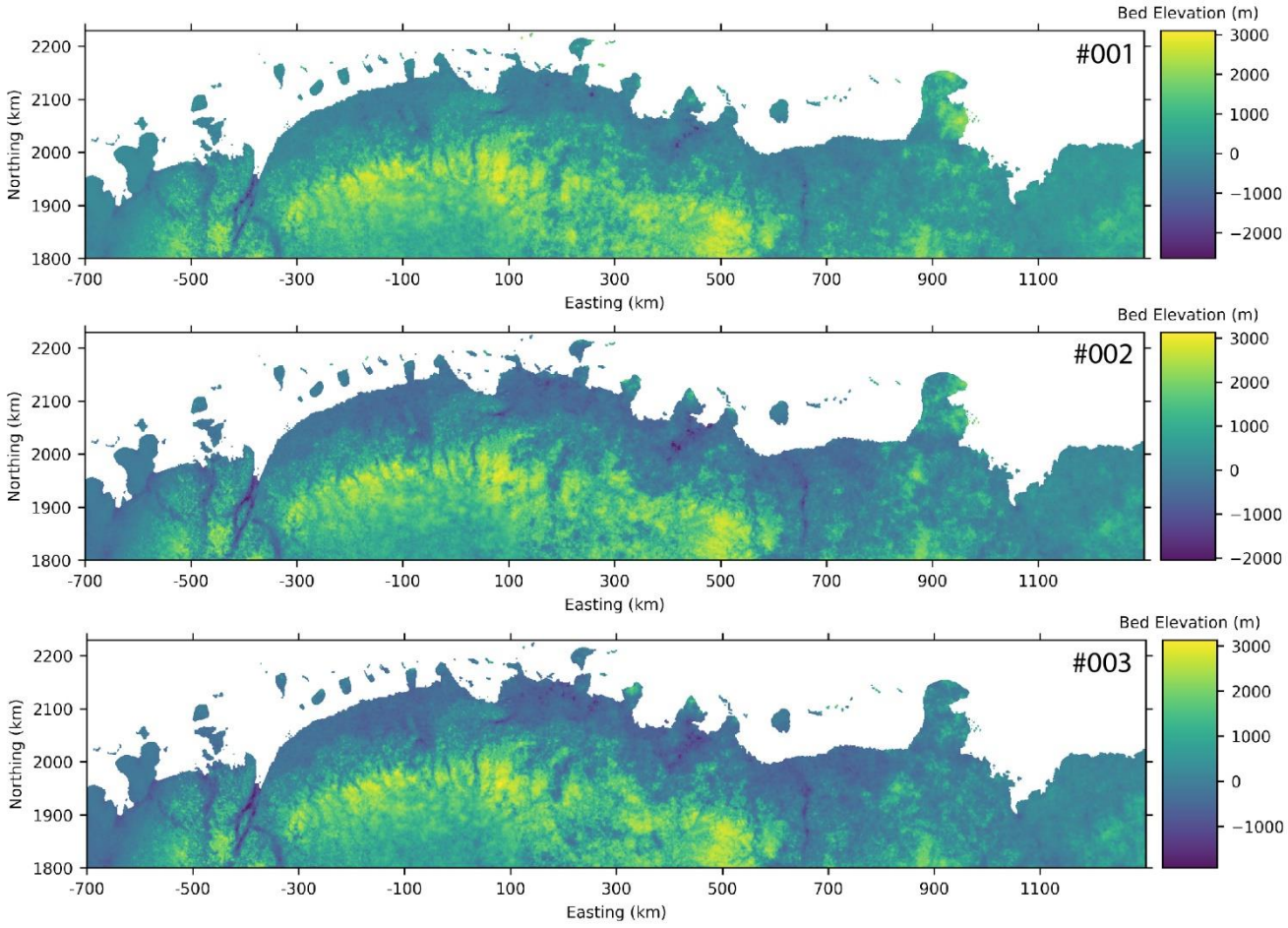

935 **Supplementary Figure 7: Example of ~~Three e~~simulated bed elevation results 001-003 out of the ensemble of 50 equally-likely grids~~xamples of simulated bed topography grids~~. Map is in a polar stereographic projection with true scale latitude of -71 and central longitude of 10 degrees.**

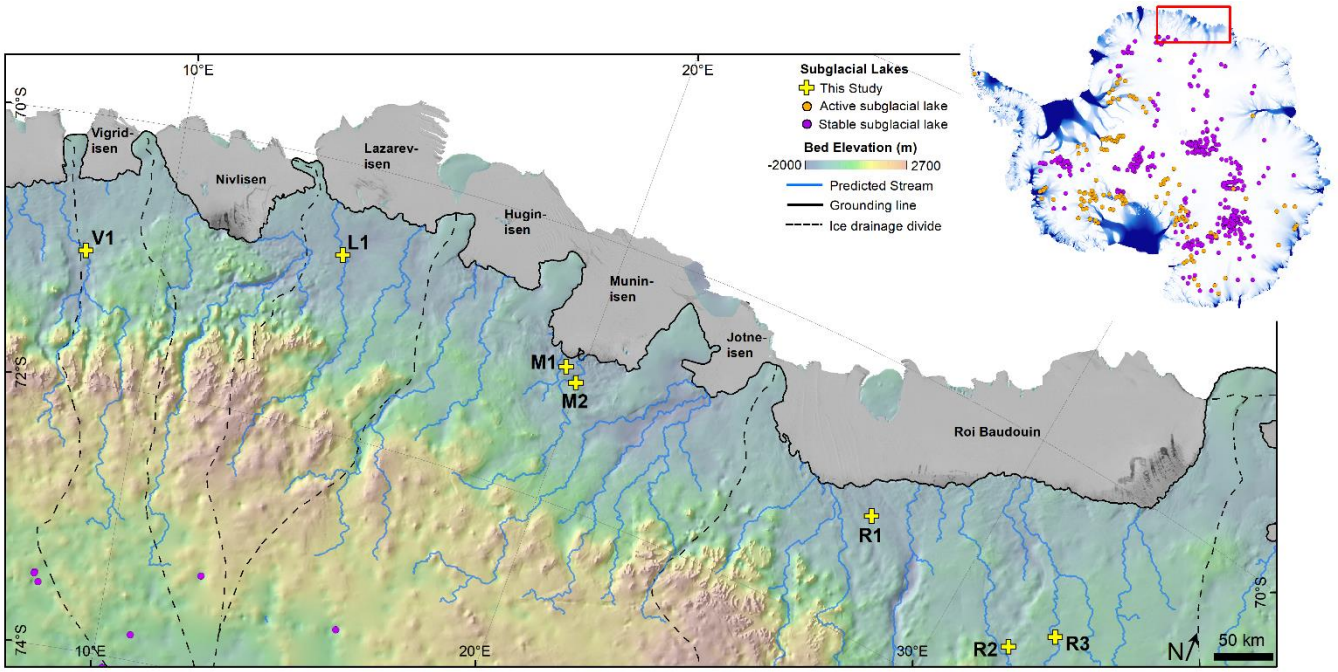

Supplementary Figure 8: Example of predicted streams from water routing analysis for one of 50 stochastic simulations. Newly-identified active lakes in this study are shown in yellow and previously -identified subglacial lakes from Goeller et al. (2016) are shown in purple. The dashed black line is the MEaSUREs grounding line (Rignot et al., 2016) and the bed elevations are from BedMachine (Morlighem et al., 2022). Ice-shelf imagery is from the MODIS mosaic (Haran et al., 2021). Subglacial lake locations depicted in the inset map are from Livingstone et al. (2022), where active lakes are represented by orange dots and stable lakes by green dots. Simulations of subglacial water drainage pathways are limited to ca. <73°.

~~**Supplementary Figure 6: Probability of subglacial drainage basin boundaries over the ensemble of 50 stochastic simulations derived from water routing analysis. The dashed black line is the MEaSUREs grounding line (Rignot et al., 2016) and ice-shelf imagery is from the MODIS mosaic (Haran et al., 2021). Subglacial lake locations depicted in the inset map are from Livingstone et al. (2022), where active lakes are represented by orange dots and stable lakes by green dots.**~~

Supplementary Table 1: Details of time-stamped 2-m REMA strips used for DEM differencing, including vertical elevation bias from co-registration with ICESat-2 (calculated as the average difference between DEM strip elevations and closest contemporaneous ICESat-2 elevations along overlapping ICESat-2 tracks), standard deviation in elevation bias and time difference between REMA strip acquisition date and the closest contemporaneous ICESat-2 elevation data. Elevation bias and time difference could not be calculated for the four last strips due to lacking contemporaneous ICESat-2 data.

REMA Strip Date	Location	Satellite	Elevation bias from ICESat-2 (m)	σ (m)	Time difference (days)
22nd October 2019	Roi Baudouin Ice Shelf	Worldview-1	-0.70	0.52	69
10th January 2021	Roi Baudouin Ice Shelf	Worldview-2	-2.41	1.20	15
18th January 2021	Roi Baudouin Ice Shelf	Worldview-1	-0.98	0.29	11
28th December 2022	Roi Baudouin Ice Shelf	Worldview-1	0.52	0.24	62
25th January 2020	Lazarev Ice Shelf	Worldview-1	3.53	0.42	12
15th February 2021	Lazarev Ice Shelf	Worldview-3	-2.10	0.42	12
12th September 2015	Lazarev Ice Shelf	Worldview-1	-		-
10th December 2016	Lazarev Ice Shelf	Worldview-1	-		-
7th December 2016	Roi Baudouin Ice Shelf	Worldview-1	-		-
21st December 2017	Roi Baudouin Ice Shelf	Worldview-1	-		-